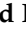





Article

Elucidation of GPR55-Associated Signaling behind THC and LPI Reducing Effects on Ki67-Immunoreactive Nuclei in Patient-Derived Glioblastoma Cells

Marc Richard Kolbe ¹, Tim Hohmann ¹ , Urszula Hohmann ¹ , Erik Maronde ² , Ralph Golbik ³, Julian Prell ⁴, Jörg Illert ⁴, Christian Strauss ⁴ and Faramarz Dehghani ^{1,*} 

- ¹ Department of Anatomy and Cell Biology, Medical Faculty, Martin Luther University Halle-Wittenberg, Grosse Steinstrasse 52, 06108 Halle (Saale), Germany; marc.kolbe@medizin.uni-halle.de (M.R.K.); tim.hohmann@medizin.uni-halle.de (T.H.); urszula.hohmann@medizin.uni-halle.de (U.H.)
- ² Department of Anatomy II, Goethe-University, Theodor-Stern-Kai 7, 60590 Frankfurt am Main, Germany; e.maronde@em.uni-frankfurt.de
- ³ Charles Tanford Protein Centre, Martin Luther University Halle-Wittenberg, Kurt-Mothes-Straße 3a, 06120 Halle (Saale), Germany; ralph.golbik@biochemtech.uni-halle.de
- ⁴ Department of Neurosurgery, Medical Faculty, Martin Luther University Halle-Wittenberg, Ernst-Grube-Str. 40, 06120 Halle (Saale), Germany; julian.prell@uk-halle.de (J.P.); joerg.illert@uk-halle.de (J.I.); christian.strauss@uk-halle.de (C.S.)
- * Correspondence: faramarz.dehghani@medizin.uni-halle.de; Tel.: +49-345-557-1707

Abstract: GPR55 is involved in many physiological and pathological processes. In cancer, GPR55 has been described to show accelerating and decelerating effects in tumor progression resulting from distinct intracellular signaling pathways. GPR55 becomes activated by LPI and various plant-derived, endogenous, and synthetic cannabinoids. Cannabinoids such as THC exerted antitumor effects by inhibiting tumor cell proliferation or inducing apoptosis. Besides its effects through CB₁ and CB₂ receptors, THC modulates cellular responses among others via GPR55. Previously, we reported a reduction in Ki67-immunoreactive nuclei of human glioblastoma cells after GPR55 activation in general by THC and in particular by LPI. In the present study, we investigated intracellular mechanisms leading to an altered number of Ki67⁺ nuclei after stimulation of GPR55 by LPI and THC. Pharmacological analyses revealed a strongly involved PLC-IP3 signaling and cell-type-specific differences in G α -, G $\beta\gamma$ -, RhoA-ROCK, and calcineurin signaling. Furthermore, immunochemical visualization of the calcineurin-dependent transcription factor NFAT revealed an unchanged subcellular localization after THC or LPI treatment. The data underline the cell-type-specific diversity of GPR55-associated signaling pathways in coupling to intracellular G proteins. Furthermore, this diversity might determine the outcome and the individual responsiveness of tumor cells to GPR55 stimulation by cannabinoids.

Keywords: calcineurin; endocannabinoid system; G $\beta\gamma$; IP3-sensitive receptor; NFAT; PLC; ROCK



Citation: Kolbe, M.R.; Hohmann, T.; Hohmann, U.; Maronde, E.; Golbik, R.; Prell, J.; Illert, J.; Strauss, C.; Dehghani, F. Elucidation of GPR55-Associated Signaling behind THC and LPI Reducing Effects on Ki67-Immunoreactive Nuclei in Patient-Derived Glioblastoma Cells. *Cells* **2023**, *12*, 2646. <https://doi.org/10.3390/cells12222646>

Academic Editor: Zhao-Hui Song

Received: 8 August 2023

Revised: 9 November 2023

Accepted: 13 November 2023

Published: 17 November 2023



Copyright: © 2023 by the authors. Licensee MDPI, Basel, Switzerland. This article is an open access article distributed under the terms and conditions of the Creative Commons Attribution (CC BY) license (<https://creativecommons.org/licenses/by/4.0/>).

1. Introduction

GPR55 is an orphan G-protein-coupled receptor (GPCR) and has been found within the central nervous system (CNS) in numerous brain regions, such as the hippocampus, striatum, cerebellum, hypothalamus, and cortex, as well as on glial cells and neurons of the dorsal root ganglia [1–5]. GPR55 is also localized outside the CNS in different organs, including the lung, pancreas, liver, spleen, and intestine [1,6–8]. Given its ubiquitous distribution, GPR55 is involved in the control of a wide spectrum of physiological processes, including endocrine function, tissue inflammation, and energy metabolism [9]. Recent data have demonstrated that GPR55 is expressed by different human tumor entities, and its activation by its ligand L- α -lysophosphatidylinositol (LPI) has tumor-promoting effects reflected by an increased tumor cell proliferation, migration, and invasion capacity [10–12].

Glioblastoma, the most common primary brain tumor, is an aggressive and highly invasive tumor characterized by inter- and intratumoral heterogeneity. Despite multimodal treatment strategies, it is considered to remain incurable. It is well discussed that the endocannabinoid system may be a promising target for the treatment of glioblastoma [13–19]. Exemplarily, phytocannabinoids Δ^9 -tetrahydrocannabinol (THC) and cannabidiol (CBD) induced cell cycle arrest [18] and apoptosis [20,21] in human glioblastoma cells. Importantly, the complexity of the pharmacology of cannabinoids and their signaling have to be characterized in more detail, allowing the development of targeted and individualized therapeutic interventions [22]. Cannabinoid-receptor 1 (CB₁) and CB₂-dependent mechanisms have been reported for anti-tumor activities of THC on glioblastoma cells [14,18–20]. However, THC and other CB₁ and CB₂ ligands can also modulate cellular responses in a CB₁/CB₂-independent manner via other receptors, including GPR55 [15,22]. GPR55 was recently postulated as a novel putative cannabinoid receptor. Among others, plant-derived and endogenous cannabinoids including THC, anandamide (AEA), 2-arachidonoylglycerol, abnormal-CBD, and LPI were found to stimulate GTP γ binding in cells stably expressing GPR55 [1,22]. Furthermore, AEA, an accepted agonist for CB₁ and CB₂, exerted anti-proliferative and pro-apoptotic effects on cholangiocarcinoma cells by activating GPR55 [23], although GPR55 is thought to promote tumor cell proliferation of other tumor entities [10–12]. These contradictory results might be explained by functional selectivity determined by cell type and ligand utilization as well as by the intracellular events downstream of GPR55 [24].

GPR55 is mainly coupled to G $\alpha_{12/13}$ [1,2,25,26] or G α_q [2]. Activation of both is associated with stimulation of multiple intracellular signaling pathways, including Ras homolog gene family member A (RhoA) and RhoA-associated protein kinase (RhoA-ROCK) pathway, phosphoinositide 3-kinase (PI3K), and phospholipase C (PLC) [1,2,25–28]. PLC can be activated directly via G α_q [2] or indirectly via PI3K [29] or RhoA/ROCK [25], resulting in hydrolysis of membrane-bound phosphatidylinositol-4,5-bisphosphate (PIP₂) to diacylglycerol (DAG) and inositol triphosphate (IP₃). Subsequently, IP₃ promotes Ca²⁺ mobilization from endoplasmic reticulum (ER) stores through IP₃-sensitive receptors [25,28]. This is followed by an activation of transcription factors by calcineurin, such as nuclear factor of activated T cells (NFAT) [25,30]. In addition, PKC and the downstream RAF/MEK/ERK cascade are activated by DAG and/or Ca²⁺ release, which is accompanied by the recruitment of other transcription factors, such as cAMP response element binding protein (CREB) and nuclear factor kappa light chain enhancers of activated B cells (NF- κ B) [28,30].

We have recently discovered that THC affected the number of Ki67-immunoreactive nuclei in human patient-derived glioblastoma cells independent of its classical target receptors CB₁ and CB₂ [16]. Interestingly, a general activation of GPR55 by its endogenous agonist LPI produced similar effects. Moreover, THC and LPI effects were abolished by specific antagonists [16]. Thus, we concluded that modulating properties of THC on Ki67-immunoreactive nuclei were driven by activation of GPR55 [16]. The present study was designed to shed light on part of the possible intracellular mechanisms downstream of GPR55 that decrease the number of Ki67 immunoreactive nuclei of human glioblastoma when these become activated by THC or LPI.

2. Materials and Methods

2.1. Cell Culture

Glioblastoma cells designated as *GBM #4* and *GBM #10* were derived from human biopsies as previously described [16]. All patients provided written informed consent. The study was conducted in accordance with the Declaration of Helsinki and was approved by the local Ethics Committee of the University Halle-Wittenberg (project reference number: 2015-144). Some molecular characteristics of the original tumor and cells under investigation are listed in Table S1 [16].

Cells were maintained in high-glucose Dulbecco's Modified Eagle Medium (Invitrogen, Schwerte, Germany, 41965-062) supplemented with 10% (*v/v*) fetal bovine serum

(FBS, Invitrogen, Schwerte, Germany, 10500-064) and 1% (*v/v*) penicillin/streptomycin (Invitrogen, Schwerte, Germany, 15140-122). The passage numbers ranged from 2 to 80.

2.2. Treatment

Either 10,000 cells for Ki67 staining or 20,000 cells for NFAT labeling were seeded on sterile coverslips (Dr. Ilona Schubert Laborfachhandel, Leipzig, Germany, 01-0012) in 24-well plates (Greiner Bio-One™, Frickenhausen, Germany, 662160). Cells were allowed to adhere overnight. They were then treated for 24 h with a fresh medium containing THC or LPI (Table 1). Following treatment, the cells were fixed using a 4% (*w/v*) paraformaldehyde solution (AppliChem, Darmstadt, Germany, 1.414.511.211). To assess effectors of GPR55-mediated signaling, cells were pre-incubated (marked as ++) with the corresponding inhibitors (Table 1) for varying durations. Subsequently, the medium was replaced by a fresh medium containing THC or LPI with or without inhibitors for 24 h. All treatments were conducted in DMEM supplemented with 10% (*v/v*) FBS. Cytotoxic effects of all inhibitors in the absence or presence of THC or LPI were assessed by viability assay (Figures S1 and S2). The concentration of inhibitors was determined based on preliminary experiments in which a range of increasing concentrations of each inhibitor was evaluated (Figures S1–S3). Notably, in cases of high inhibitor concentrations, alternate signaling routes might become activated and induce additional off-target effects.

Table 1. Substances.

Substances	Targets	Behavior	Solvent	Concentration	Pre-Incubation Time	Company	Article Number
2-APB	IP3-sensitive receptors	inhibitor	DMSO	10 μ M	30 min [28]	Tocris, Bristol, UK	1224
cyclosporine A (CsA)	calcineurin	inhibitor	DMSO	0.1 μ M 1 μ M	1 h [31]	Tocris, Bristol, UK	1101
Dronabinol (THC)	CB ₁ CB ₂ GPR18 GPR55	agonist [22]	DMSO	5 μ M	-	THC pharm GmbH, Frankfurt am Main, Germany	THC-1016
FK506	calcineurin	inhibitor	DMSO	0.5 μ M 5 μ M	1.5 h [32]	Tocris, Bristol, UK	3631
forskolin	adenylyl cyclase	activator	DMSO	0.1 μ M 1 μ M 5 μ M 10 μ M 30 μ M	-	Sigma, Darmstadt, Germany	
gallein	G β γ -subunits	inhibitor	DMSO	10 μ M	15 min [33]	Tocris, Bristol, UK	3090
ionomycin	-	calcium ionophore	DMSO	10 μ M	-	Tocris, Bristol, UK	1704
lysophosphatidyl-inositol (LPI)	GPR55	agonist [34]	DMSO	1 μ M	-	Sigma, Darmstadt, Germany	L7635
pertussis toxine (PTX)	G _{i/o} -proteins	inhibitor	H ₂ O	100 ng/ml	16 h [35]	Tocris, Bristol, UK	3097
U73122	PLC	inhibitor	DMSO	0.1 μ M	15 min [36]	Cayman Chemicals, Ann Arbor, Michigan, USA	70740

Table 1. Cont.

Substances	Targets	Behavior	Solvent	Concentration	Pre-Incubation Time	Company	Article Number
U73343	-	inactive analogue of U73122	DMSO	0.1 µM	15 min	Tocris, Bristol, UK	4133
thapsigargin	SERCA	inhibitor	DMSO	2 µM	-	Tocris, Bristol, UK	1138
Y-27632	ROCK	inhibitor	H ₂ O	10 µM	1 h [37]	Tocris, Bristol, UK	1254

2.3. 3-(4,5-Dimethylthiazol-2-yl)-2,5-Diphenyl-Tetrazolium Bromide (MTT)-Viability-Assay

A total of 3000 cells were placed in 96-well plates (Greiner Bio-One™, Frickenhausen, Germany, 650160) and allowed to adhere overnight. Cells were treated with inhibitors at concentrations specified in Table 1 for 24 h. Four hours before termination of experiments, 3-(4,5-dimethylthiazol-2-yl)-2,5-diphenyltetrazolium bromide solution (MTT, Invitrogen, Schwerte, Germany, M6494) at a concentration of 5 mg/mL was added and incubated for 4 h at 37 °C and 5% (v/v) CO₂. After removing the MTT solution, formazan crystals within the cell bodies were dissolved using 100 µL of dimethyl sulfoxide (DMSO, Sigma, Darmstadt, Germany D4540). Absorbance values (Ab) were measured at 540 nm and 720 nm using a microplate reader (SynergyTMMx, BioTek Instruments, Winooski, VT, USA). Control groups consisted of cells incubated in media free of inhibitors, whereas media without cells served as blanks. Cell viability was calculated as follows:

$$\text{viability}[\%] = \frac{(Ab_{\text{treated}}^{520\text{nm}} - Ab_{\text{treated}}^{720\text{nm}}) - (Ab_{\text{blank}}^{520\text{nm}} - Ab_{\text{blank}}^{720\text{nm}})}{(Ab_{\text{untreated}}^{520\text{nm}} - Ab_{\text{untreated}}^{720\text{nm}}) - (Ab_{\text{blank}}^{520\text{nm}} - Ab_{\text{blank}}^{720\text{nm}})} \times 100 \quad (1)$$

All experiments were performed independently at least three times with six technical replicas for each treatment group.

2.4. PCR

Total RNA extraction was performed using peqGOLD Trifast™ (Peqlab, Erlangen, Germany, 30-2010). Extracts were treated with a DNA-free™ Kit (Invitrogen, Schwerte, Germany, AM1906) according to the manufacturer's instructions. RNA concentration was quantified using a Synergy™ Mx Microplate Reader (SynergyTMMx, BioTek Instruments, Winooski, VT, USA). PCR amplification was conducted with 4 µL generated cDNA (Reverse Transcription System, Thermo Fisher Scientific, Waltham, MA, USA, K1691) in 20 µL volume containing 10 µL PCR-MasterMix (Promega Inc., Madison, WI, USA, M7505), 0.5 µL forward and 0.5 µL reverse primer (25 pM), 0.25 µL of EvaGreen dye (Biotium, Fremont, CA, USA, 31000), and 4.75 µL of nuclease-free water (Promega Inc., Madison, WI, USA, P1193). The PCR reaction was performed for 40 cycles using a PCR cycler (7900HT Fast Real-Time PCR System, Applied Biosystems™, Thermo Fisher Scientific, Waltham, MA, USA). Conditions used were as follows: initial denaturation at 95 °C, followed by 40 cycles of denaturation at 94 °C (3 s), annealing at 60 °C, elongation at 72 °C (30 s), and fluorescence detection at 76 °C (*GNA13*, *GNAQ*, *GNAI1*, *GAPDH*, *TPB*) or 80 °C (*GNA12*, *GNAO1*, *GNAI2*, *GNAI3*, *GNASS*, *GNASL*, *POLRR2A*) (15 s). For visualization of PCR products, 30 PCR cycles were performed. Products were separated by electrophoresis on 1.5% (w/v) agarose gels (PeqLab, Erlangen, Germany, 35-1020) containing GelRed (Biotium, Fremont, CA, USA, 41003) and were visualized using BioTek Synergy Mix (BioTek Instruments, Winooski, VT, USA) (Figure S5). The primers used are listed in Table 2. Relative transcript levels were calculated using the 2^{-ΔΔCt} method. For normalization, RNA polymerase II subunit A (*POLR2A*) served as an internal reference. Normalization to glyceraldehyde-3-phosphate

dehydrogenase (*GAPDH*) and TATA-binding protein (*TBP*) were performed to ensure validity and reproducibility as well as to show stable expression of used reference genes in the experimental setup (Figures S6 and S7).

Table 2. Primers.

Gene	Accession Number	Forward Primer (5' → 3')	Reverse Primer (5' → 3')	Size [bp]
<i>GAPDH</i>	NM_002046	TGCACCACCAACTGCTTAGC	GGCATGGACTGTGGTCATGAG	87
<i>GNA12</i>	NM_007353	GAGCTCTGCAGGTGTGGATT	GAAGATGGGAGAGCCGTCTG	226
<i>GNA13</i>	NM_006572	CGTCGAGAATTTCAACTGGGTG	CTTTGGTGGGTCTTCTGGCA	121
<i>GNAI1</i>	NM_002069	GCTGAAGATGAAGAAATGAACCGAA	GTCCCAGATGCATTTGCCTT	481
<i>GNAI2</i>	NM_002070	CAGGCAGCTATTTGCACTGTC	AGGTCGTTCAAGTAGTAGGC	168
<i>GNAI3</i>	NM_006496	AGTTTCCGTGGTGTGAGTGA	GATTCTCCAGCACCCGAGTAGC	184
<i>GNAO1</i>	NM_020988	TGGTGATAAGGAGAGAAAGGCTG	TCGTTGAGCTGATACTCCCG	168
<i>GNAQ</i>	NM_002072	TGAGACAATAAGGCTCATGC	ATCTTGTTGCGTAGGCAGGT	226
<i>GNASL</i>	NM_000516	GAGCAACAGCGATGGTGAGA	TGATCGCTCGGCACATAGTC	342
<i>GNASS</i>	NM_080426	GCAGAAGGACAAGCAGGTCTA	TTGGTTGCCTTCTCACTGTCTC	141
<i>POLR2A</i>	NM_000937	CTTGCCCCGTGCCATGCAGA	CTCGCACCCGGCCTTCCTTG	83
<i>TBP</i>	NM_003194	GAGCTGTGATGTGAAGTTTCC	TCTGGGTTTGATCATTCTGTAG	117

2.5. Immunochemical Staining of Ki67

Endogenous peroxidase activity was blocked by 3% (*v/v*) H₂O₂ (Roth, Karlsruhe, Germany, 8070.2) in methanol (Roth, Karlsruhe, Germany, AE01.2) for 10 min. Subsequently, cells were washed three times with 0.02 M PBS containing 0.3% (*v/v*) Triton X-100 (AppliChem, Darmstadt, Germany, A1388.0500) (PBS/Triton). To minimize unspecific binding, normal goat serum (NGS) (Merck, Darmstadt, Germany, S26) was used at a dilution of 1:20. Cells were incubated overnight at room temperature with primary antibodies (Table 3) appropriately diluted in 0.02 M PBS containing 0.5% (*w/v*) bovine serum albumin (BSA) (Sigma, Darmstadt, Germany, A7906) and 0.3% (*v/v*) Triton X-100. After rinsing with PBS/Triton, cells were treated with a goat anti rabbit-specific biotinylated secondary antibody for 1 h at room temperature (Table 3). After incubation with ExtrAvidin[®] peroxidase (Sigma, Darmstadt, Germany, E2886) for 1 h, diaminobenzidine (Sigma, Darmstadt, Germany, D8001) was added together with 0.05% (*v/v*) H₂O₂ for 3 min. Meyer's hematoxylin (Hollborn und Söhne GmbH, Leipzig, Germany, H02-0500) was used to counterstain the cell nuclei. Cells were dehydrated in an ascending concentration gradient of ethanol, cleaned with xylene (Roth, Karlsruhe, Germany, 97.13.3), and embedded in Entellan (Merck, Darmstadt, Germany, 107960).

Table 3. Antibodies.

Antibodies	Species	Concentration (Application)	Company	Article Number
anti-Ki67	rabbit	1:200 (ICC)	DSC innovative Diagnostic-System, Hamburg, Germany	KI681C002
anti-NFAT1	rabbit	1:200 (IF)	Cell Signaling, Danvers, MA, USA	5861
anti-NFAT2	rabbit	1:200 (IF)	Invitrogen, Schwerte, Germany	PA5-90432
anti-NFAT3	rabbit	1:200 (IF)	Invitrogen, Schwerte, Germany	PA1-021
anti-NFAT4	rabbit	1:200 (IF)	Invitrogen, Schwerte, Germany	PA5-99546
anti-rabbit Alexa488 conjugated	goat	1:200 (IF)	Invitrogen, Schwerte, Germany	A11034
anti-rabbit IgG, biotin conjugated	goat	1:100 (ICC)	Sigma, Darmstadt, Germany	B7389

Staining was visualized by using a Leica DMi8 microscope (Leica, Wetzlar, Germany) at 200× magnification. A total of five different regions on each coverslip were captured. Ki67-positive (Ki67⁺) and hematoxylin-positive cells were counted manually, and the ratios of Ki67⁺ nuclei were determined as previously described [16].

2.6. Immunofluorescence Labeling of NFAT

Fluorescence labeling was performed to determine subcellular localization of NFAT isoforms 1–4 after THC or LPI stimulation at different time points (5 min, 10 min, 30 min, 2 h, 4 h, and 24 h). Fixed cells were permeabilized with PBS/Triton for 10 min, followed by incubation with NGS (1:20 in PBS/Triton) for 30 min, before the primary antibody (Table 3) was diluted in 0.5% (*w/v*) BSA and PBS/Triton was applied overnight at room temperature. Cells were washed with PBS/Triton and treated for 60 min with Alexa488-labeled secondary antibody (Table 3). Nuclei were counterstained with DAPI (Sigma, Darmstadt, Germany, D5637) for 5 min. Coverslips were mounted on slides with a fluorescent mounting medium (Dako, Jena, Germany, S3023). Images of fixed cells were acquired at 400× magnification using a confocal laser scanning microscope (Leica TCS SPE, Wetzlar, Germany). The following excitation wavelengths were used: 405 nm for DAPI and 488 nm for NFAT isoforms. Emission was detected in the range of $\Delta\lambda = 415\text{--}480$ nm (DAPI) and $\Delta\lambda = 500\text{--}570$ nm (NFAT).

2.7. Statistics

The values were presented as means with standard errors of the mean derived from at least three independent experiments. Because of an uneven number of values, one of the replicas could not be evaluated due to a very low number of assessable cells on the coverslips. All experimental groups were normalized to the untreated control group. Statistical analyses were conducted using either Student's *t*-test or the one-way ANOVA with Tukey's post hoc test in GraphPad Prism9 (version. 9.4.1, Boston, MA, USA). The analysis for the normal distribution was performed using the Shapiro–Wilk normality test. All *p*-values referred to the corresponding untreated group or to the group treated with the inhibitor for the relevant effector. Differences were considered significant at $p \leq 0.05$.

3. Results

As LPI, a specific activator of GPR55, reduced the number of Ki67⁺ nuclei via GPR55 to a similar extent as THC under comparable experimental conditions [16], LPI was used as a positive control to demonstrate GPR55-specific signaling. Downstream signaling pathways of GPR55 were investigated after THC or LPI exposure by using inhibitors and antagonists of various intracellular effectors.

3.1. Cell-Type-Specific ROCK Signaling and a Strongly Involved PLC-IP3 Signaling

To further confirm GPR55-dependent signaling of THC and LPI, we first evaluated the involvement of known key effectors associated with GPR55 pathways. RhoA and its downstream effector ROCK have recently been implicated as key effectors in GPR55-mediated signaling [25]. As many of the cellular actions of RhoA are mediated by ROCK, the effects of ROCK inhibitor Y-27632 were investigated on THC and LPI responses. In *GBM #10*, the addition of Y-27632 markedly blocked THC- and LPI-mediated changes in the ratio of Ki67⁺ cells (Figures 1a,b, S3a and S4a, Table S2). Interestingly, in *GBM #4*, ROCK was not involved since effects of THC or LPI were still observed in the presence of Y-27632 (Figures 1a,b, S3a and S4a, Table S2). These data indicate a cell-type-specific impact of THC and LPI on the number of Ki67⁺ nuclei via RhoA/ROCK-dependent signaling.

PLC has been shown to be another important part of signaling pathways triggered by GPR55 [2,25,36,38]. Thus, cells were treated with PLC inhibitor U73122. U73122 significantly diminished THC effects in *GBM #4* and *GBM #10* (Figures 2a and S3b, Table S3). Similar results were obtained for LPI, as LPI's effects were no longer detected in the presence of U73122 (Figures 2b and S4b, Table S3). The specificity of U73122 to block PLC was confirmed by using its inactive structural analogue U73343 at the same concentrations used for U73122. Indeed, treatment with U73343 failed to block the responses to THC and LPI in both glioblastoma cell lines (Figure 2a,b, Table S4). U73122 and U73343 themselves displayed no significant effects on the number of Ki67⁺ nuclei (Figures 2a,b, S3b and S4b,

Tables S3 and S4). These data indicate that PLC is strongly involved in the regulation of the number of Ki67⁺ nuclei by THC and LPI in both *GBM #4* and *GBM #10*.

PLC converts membrane-bound PIP₂ to DAG and IP₃. Subsequently, IP₃ acts as a second messenger and binds to IP₃-sensitive receptors on the ER, resulting in an increase in intracellular Ca²⁺ concentrations. To assess whether IP₃ and its receptor were involved in the reduction of Ki67⁺ nuclei upon THC or LPI exposure, we used 2-APB to antagonize IP₃-sensitive receptors (Figures 3a,b, S3c and S4c, Table S5). Pretreatment with 2-APB attenuated the responses to THC and LPI in both *GBM #4* and *GBM #10* (Figures 3a,b, S3c and S4c, Table S5), making the participation of IP₃-mediated signaling downstream of GPR55 evident and further confirming PLC-dependent signaling.

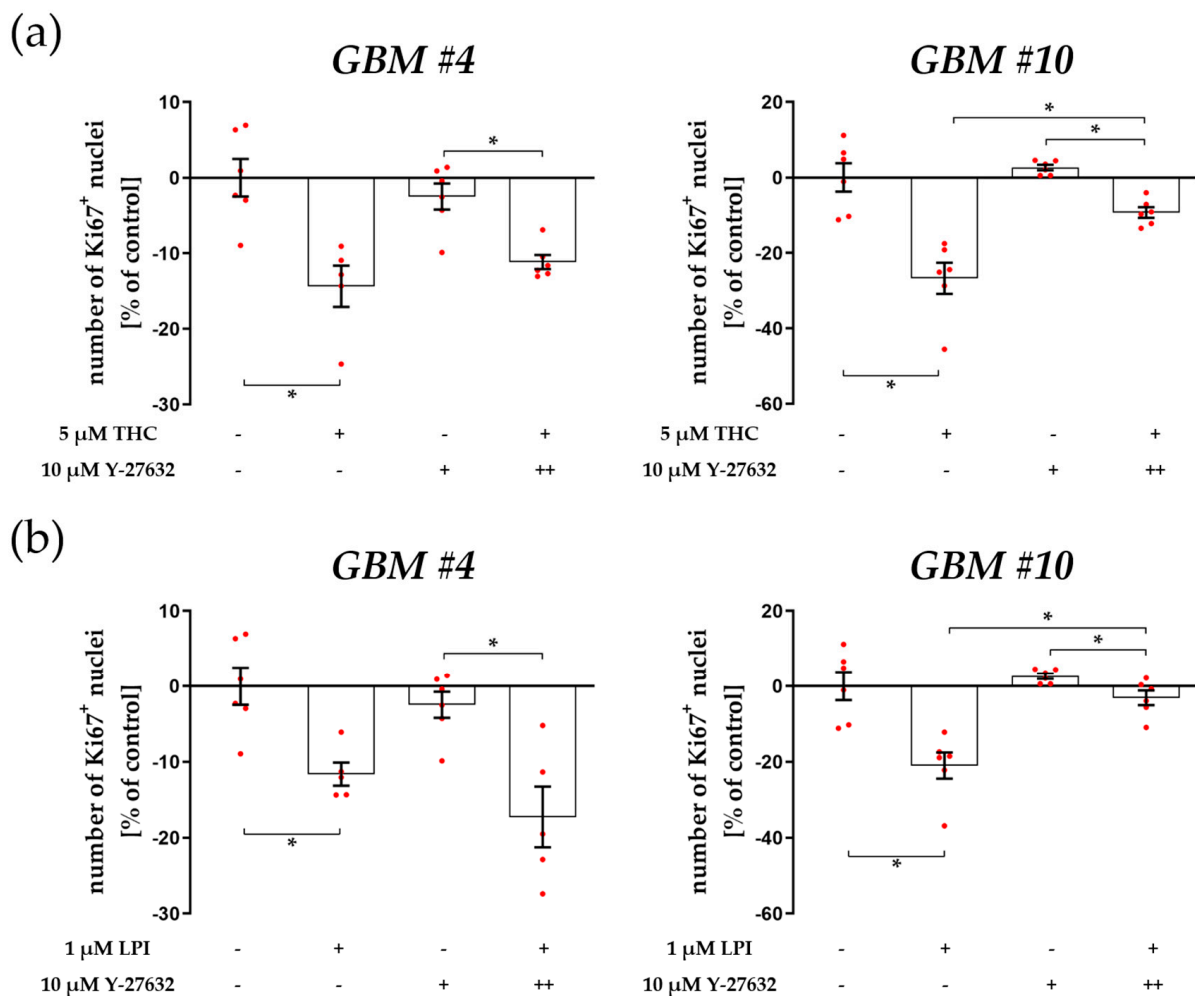


Figure 1. Impact of ROCK inhibitor Y-27632 on THC- and LPI-induced reduction of the number of Ki67⁺ nuclei. *GBM #4* and *GBM #10* were left untreated or exposed to THC (a) or LPI (b) for 24 h, resulting in a decreased number of Ki67⁺ nuclei. In *GBM #4* THC- (a) and LPI (b)-mediated effects on the number of Ki67⁺ nuclei remained unaffected in the presence of Y-27632. In contrast, pretreatment with Y-27632 significantly attenuated the responses of *GBM #10* to THC (a) and LPI (b). Altered numbers of Ki67⁺ nuclei by Y-27632 itself were not observed (a,b). Data are presented as means ± SEMs of N = 3 independent experiments performed in duplicate. Each red dot represents an individual data point. −/+ indicates without/with the corresponding substance. ++ denotes that cells were pre-incubated with Y-27632 before THC or LPI was added. Significance was set at $p < 0.05$. The asterisk denotes significant results regarding the respective measurement indicated by the bar.

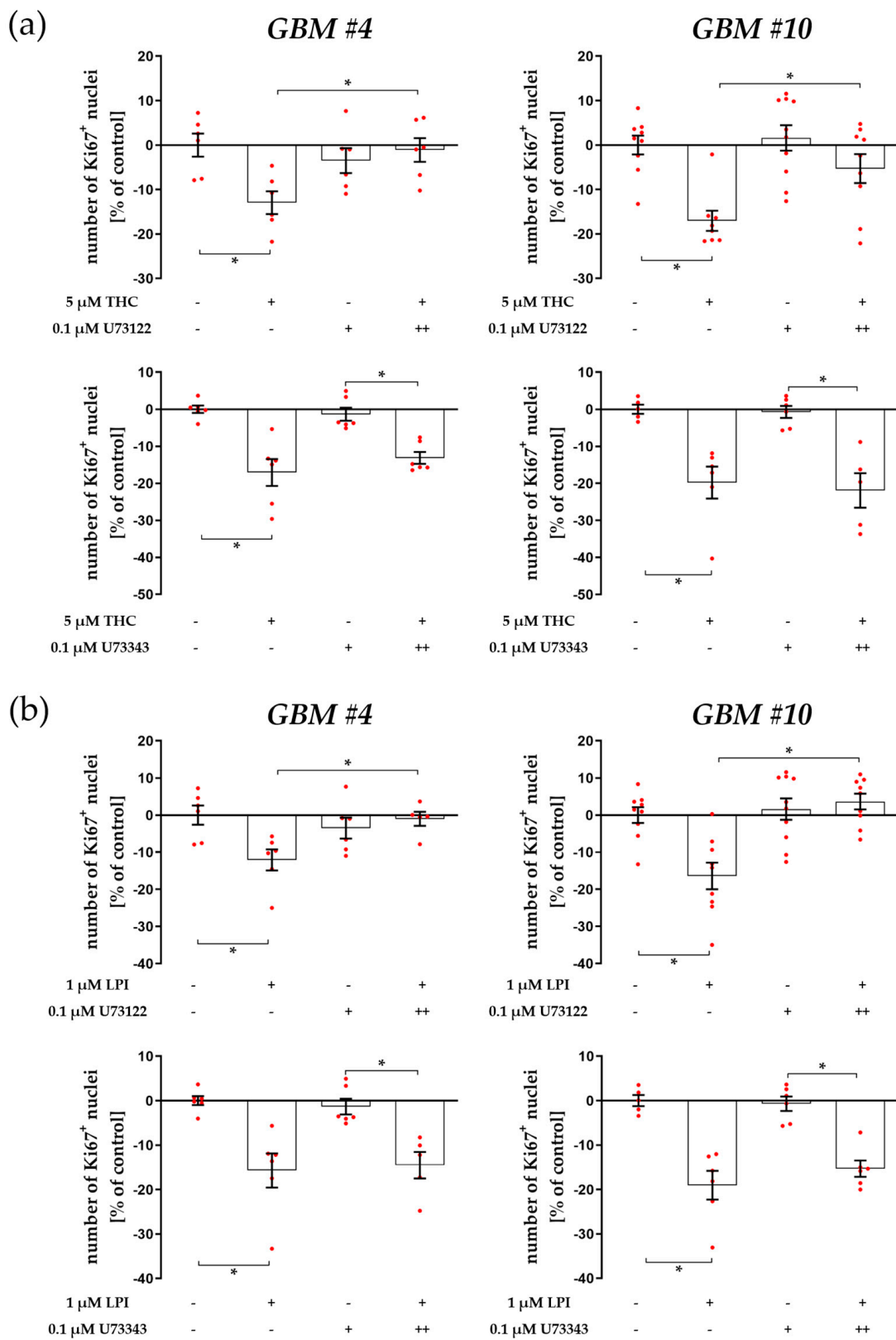


Figure 2. Impact of PLC inhibitor U73122 and its inactive analogue U73343 on THC- and LPI-induced reduction of the number of Ki67⁺ nuclei. GBM #4 and GBM #10 were left untreated or exposed to THC (a) or LPI (b) for 24 h, resulting in a decreased number of Ki67⁺ nuclei. Pretreatment with U73122, a commonly used inhibitor of PLC, significantly reversed the effects obtained after exposure to THC (a) or LPI (b) in both GBM #4 and GBM #10. Its inactive form U73343 failed to diminish the

responses to THC (a) and LPI (b) at the same concentrations used for U73122. U73122 or U73343 alone did not cause any alterations (a,b). Data are presented as means \pm SEMs of N = 3 independent experiments performed in duplicate. Each red dot represents an individual data point. -/+ indicates without/with the corresponding substance ++ denotes that cells were pre-incubated with U73122 or U73343 before THC or LPI was added. Significance was set at $p < 0.05$. The asterisk denotes significant results regarding the respective measurement indicated by the bar.

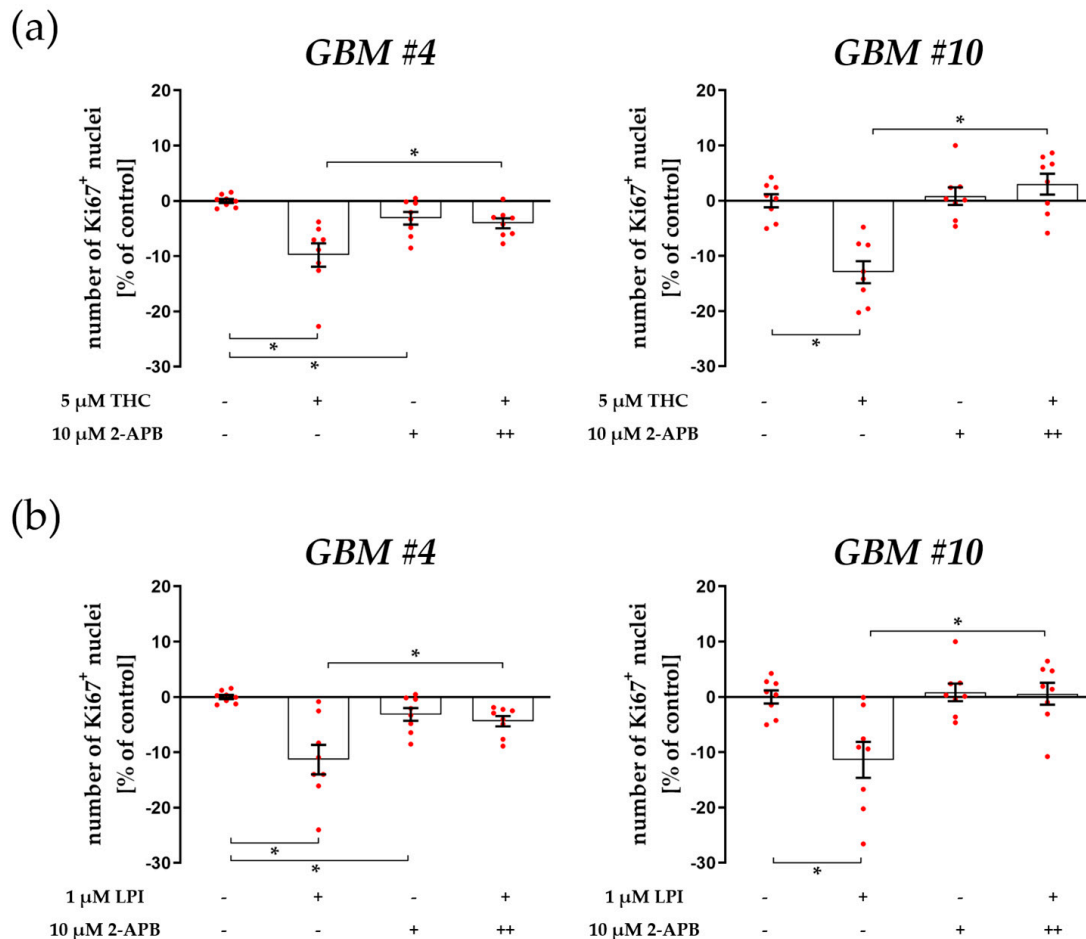


Figure 3. Impact of antagonized IP3-sensitive receptors using 2-APB on THC- and LPI-induced reduction of the number of Ki67⁺ nuclei. *GBM #4* and *GBM #10* were left untreated or exposed to THC (a) or LPI (b) for 24 h, resulting in a decreased number of Ki67⁺ nuclei. The effects of THC (a) and LPI (b) were significantly reduced after pre-incubation with 2-APB in both *GBM #4* and *GBM #10*. When *GBM #4* was exposed to 2-APB alone, a small reduction in the number Ki67⁺ nuclei were observed (a,b). Data are means \pm SEMs of N = 4 independent experiments performed in duplicate. Each red dot represents an individual data point. -/+ indicates without/with the corresponding substance. ++ denotes that cells were pre-incubated with 2-APB before THC or LPI was added. Significance was set at $p < 0.05$. The asterisk denotes significant results regarding the respective measurement indicated by the bar.

3.2. Characterization of $G\alpha$ - and $G\beta\gamma$ -Subunits, Which Might Couple to GPR55 Signaling

In light of the diversity of G proteins and their functions, the expression of different G-protein α subunits and their isoforms were examined by qRT-PCR analysis of untreated glioblastoma cells. Our results demonstrated that $G\alpha_o$, $G\alpha_i$ (isoforms 1, 2, and 3), $G\alpha_s$ (small and large isoforms), $G\alpha_{12}$, $G\alpha_{13}$, and $G\alpha_q$ were expressed by *GBM #4* and *GBM #10* at different levels. It is well known that GPR55 can be coupled to the $G\alpha_{12/13}$ and $G\alpha_q$ proteins. Both subunits were found in *GBM #4* and *GBM #10* at different levels of transcription (Figures 4a,b, S5 and S6). Remarkably, $G\alpha_q$ was highly expressed by *GBM*

#10 when compared to GBM #4, leading to an altered expression abundance of *GNAQ* compared to other transcripts of $G\alpha$ subunits (Figures 4b and S7). As PLC-dependent and RhoA/ROCK-independent signaling were observed in GBM #4 (Figures 1a,b, 2a,b, S3a–c and S4a–c, Tables S2–S4), $G\alpha_q$ -mediated signaling by GPR55 was assumed. In contrast, in GBM #10, both RhoA/ROCK- and PLC-dependent signaling (Figures 1a,b, 2a,b, S3a–c and S4a–c, Tables S2–S4) were suggested via $G\alpha_{12/13}$ and/or $G\alpha_q$ proteins.

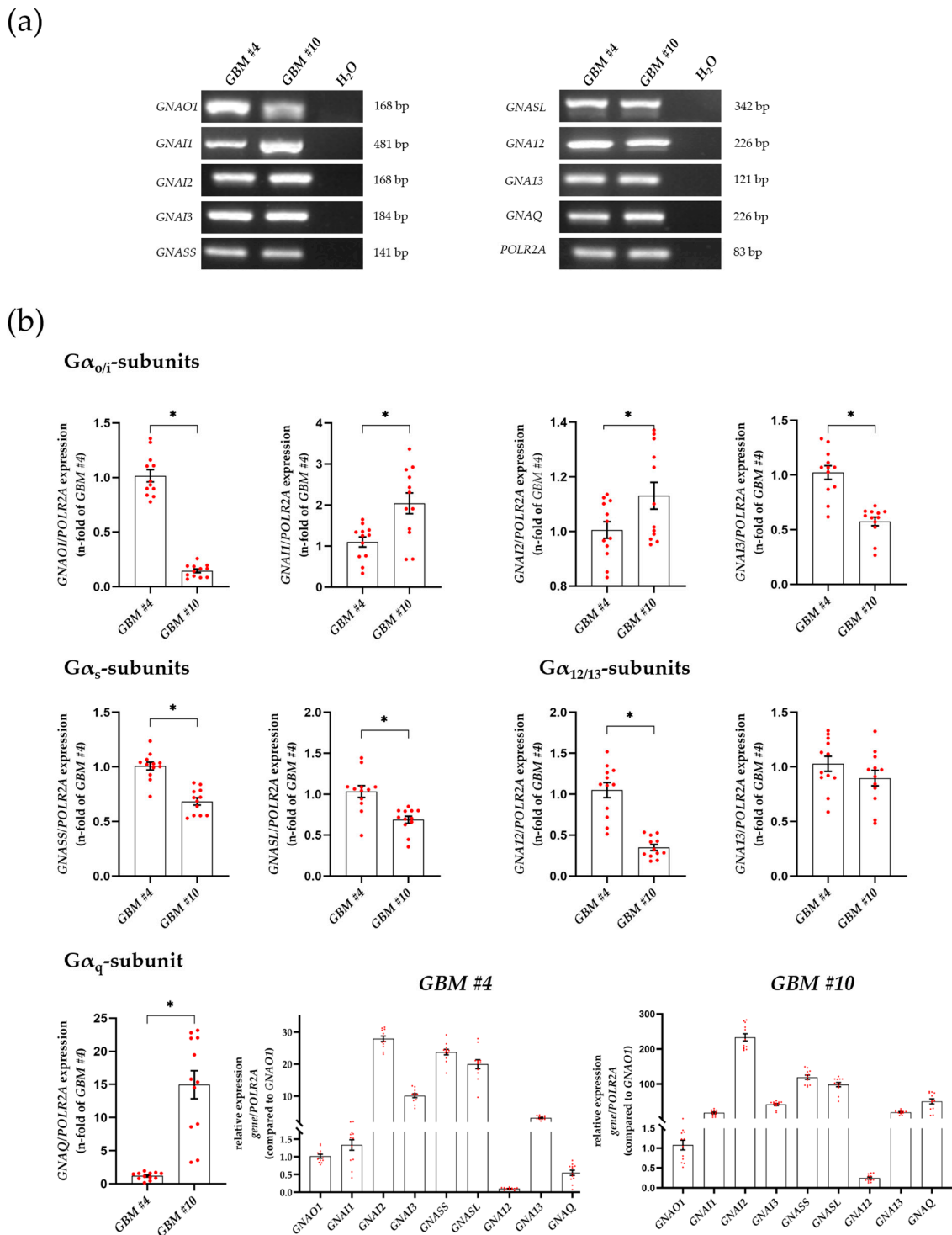


Figure 4. Detection and quantification of genes encoding different $G\alpha$ subunits at transcript level. Expression of *GNAO1*, *GNAI1*, *GNAI2*, *GNAI3*, *GNASS*, *GNASL*, *GNA12*, *GNA13*, and *GNAQ* were

analyzed by quantitative RT-PCR in untreated cells of *GBM #4* and *GBM #10*. All cells expressed the examined $G\alpha$ -subunits as transcripts (a) at different levels (b). *RNA polymerase II subunit A (POLR2A)* served as an internal reference. Furthermore, relative transcript levels were calculated using the $2^{-\Delta\Delta C_t}$ method (b). Remarkably, *GBM #4* showed a significantly higher amount of $G\alpha_o$ transcripts than *GBM #10*, whereas $G\alpha_q$ showed significantly higher expression by *GBM #10* when compared to *GBM #4*. The abundance and distribution of gene transcripts encoding different subunits within one cell population were similar in *GBM #4* and *GBM #10*. Altered ratios to others were observed for *GNAOI* in *GBM #4* and *GNAQ* in *GBM #10*. Data represent means \pm SEMs (normalized to *GBM #4* or *GNAOI*) of $N = 4$ independent experiments performed in triplicate. Each red dot represents an individual data point. Significance was set at $p < 0.05$. The asterisk denotes significant results regarding the respective measurement indicated by the bar.

According to heterodimerization with other GPCRs, including CB_1 and CB_2 , GPR55 might also activate other intracellular G-proteins such as $G\alpha_{i/o}$ indirectly. Notably, *GBM #4* showed a significantly higher amount of $G\alpha_o$ transcripts than *GBM #10*, leading to an altered expression abundance of *GNAOI* compared to other G-protein transcripts (Figure 4b). The involvement of $G\alpha_{i/o}$ proteins as reported for CB_1/CB_2 -dependent signaling was examined using the pertussis toxin (PTX), which inhibits the coupling of $G\alpha_{i/o}$ proteins to their cognate GPCRs. PTX was unable to block actions of THC and LPI in *GBM #4* and *GBM #10*. Notably, PTX (100 ng/mL) displayed by itself an altered number of Ki67⁺ nuclei (Figure 5a,b, Table S8). Furthermore, no additive agonistic or antagonistic effects of PTX and THC or LPI were observed (Figure 5a,b, Table S8). Since blocking the $G\alpha_{i/o}$ proteins with PTX leads to unhindered activation of adenylyl cyclase (AC), the increased AC activity was assumed to be responsible for the reduced number of Ki67⁺ nuclei after PTX treatment. To clarify the role of activated AC, increasing concentrations of forskolin (FSK) were applied (Figure 5c, Table S9). FSK reduced the number of Ki67⁺ nuclei in a concentration-dependent manner in *GBM #4* and *GBM #10*. The data confirm the participation of an increased AC activity in reducing the number of Ki67⁺ nuclei after PTX treatment that is independent of GPR55.

Since GPCRs have the capacity to produce signals through the actions of liberated $G\alpha$ and $G\beta\gamma$ subunits, we further examined the involvement of $G\beta\gamma$ subunits. Targeting $G\beta\gamma$ subunits by gallein, a small molecule that binds to $G\beta\gamma$ and disrupts $G\beta\gamma$ signaling, significantly reversed the decreased number of Ki67⁺ nuclei elicited by THC in *GBM #4* (Figures 6a and S3d, Table S10). In contrast, THC's effect on *GBM #10* remained unaffected in the presence of gallein (Figures 6a and S2d, Table S10). Similar results were obtained for LPI, as gallein attenuated the response to LPI in *GBM #4*, but not in *GBM #10* (Figures 6b and S4d, Table S10). The data suggest that $G\beta\gamma$ -dependent (*GBM #4*) and $G\beta\gamma$ -independent (*GBM #10*) signaling might follow an activation of GPR55 by THC or LPI.

3.3. Cell-Type-Specific Calcineurin Signaling and an Unaltered Subcellular Localization of NFAT

Well-established downstream effects of GPR55-driven PLC-IP3 signaling include an increase in intracellular Ca^{2+} concentrations and the Ca^{2+} -dependent activation of calcineurin. Cyclosporine A (CsA) and FK506 were therefore used to bind to calcineurin and inhibit its phosphatase activity by forming complexes with immunophilins. In *GBM #4*, CsA and FK506 significantly attenuated the reduced number of Ki67⁺ nuclei after THC or LPI treatment (Figures 7a,b, S3e,f and S4e,f, Tables S11 and S12). Notably, CsA treatment itself led to a decreased number of Ki67⁺ nuclei but to a smaller extent than observed for THC or LPI (Figures 7a,b and S3e,f, Table S11). In contrast, in *GBM #10*, the effects of THC and LPI were not affected by CsA but were inhibited by FK506. It should be noted that in *GBM #10*, lower concentrations of CsA and FK506 had to be used as compared to *GBM #4*.

Next, we tested the ability of GPR55 activation by THC and LPI to induce NFAT as an example of a Ca^{2+} /calcineurin-dependent regulator of transcription. Given that NFAT5 is generally associated with responses to osmotic stresses independently of calcineurin, its role in response to THC and LPI was not examined. Calcineurin-dependent dephos-

phorylation of NFAT promotes the translocation of cytoplasmic NFAT into the nucleus to initiate or repress transcription of NFAT-specific genes. Resident inactive NFAT is localized within the cytoplasm, whereas dephosphorylated, activated NFAT is found in the nucleus. However, NFAT1-4 was detected in the nucleus and cytoplasm of *GBM #4* and *GBM #10* (Figures 8 and 9). Subcellular localization of different NFAT isoforms was visualized by fluorophore labeling (Figures 8 and 9). In untreated control cells, NFAT1, NFAT2, and NFAT4 were mainly detected in the cytoplasm (Figures 8 and 9). NFAT1 and NFAT2 at low basal levels and NFAT3 at high levels were also localized in the nucleus. In contrast, NFAT4 was observed solely in the cytoplasm (Figure 9b). Stimulation with THC or LPI did not produce significant changes in the nuclear signals of NFAT1, NFAT2, NFAT3, or NFAT4 in *GBM #4* and *GBM #10* after 5 min, 10 min, 30 min, 2 h, 4 h, or 24 h (NFAT1 in *GBM#4* Figure S8).

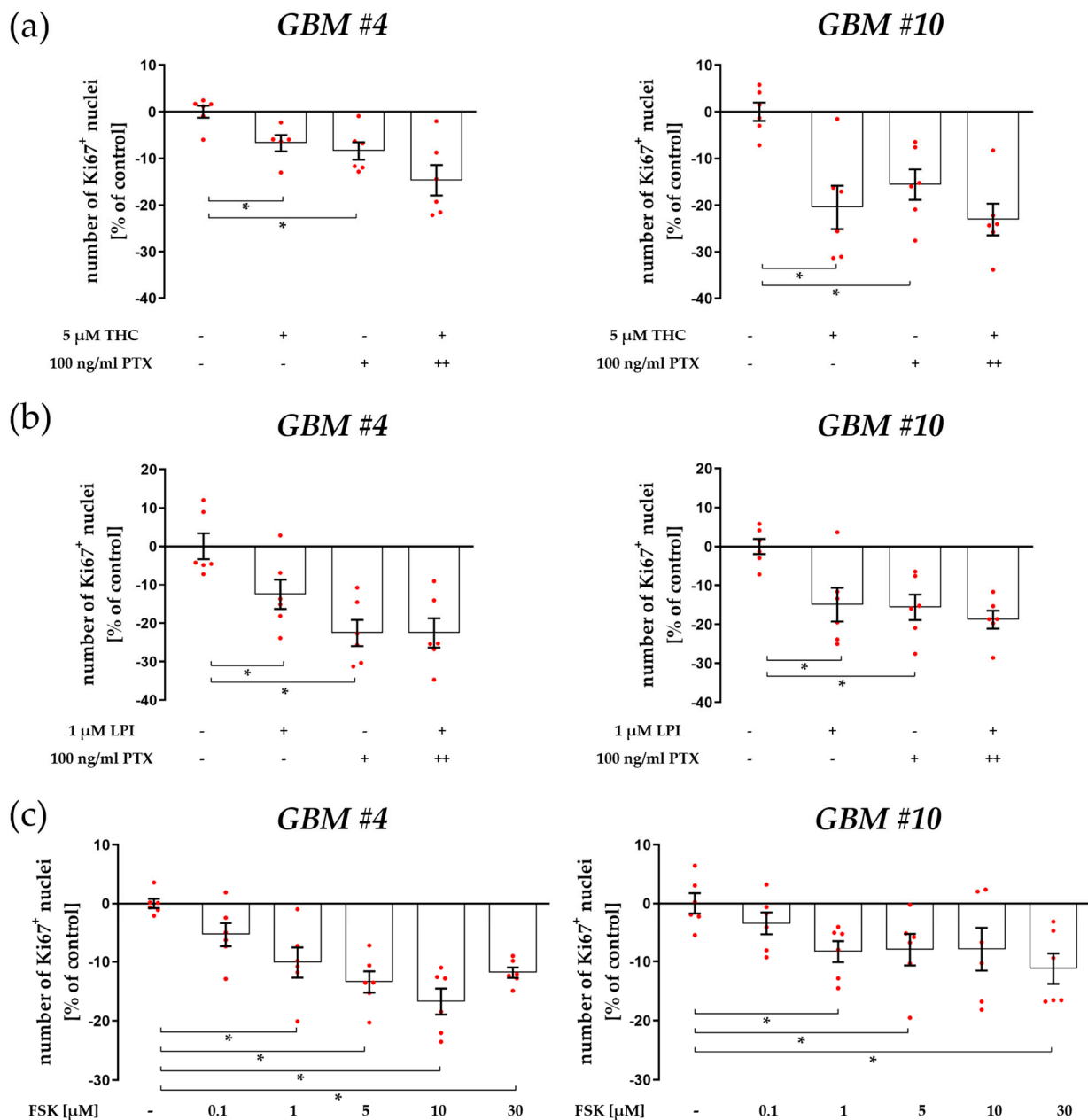


Figure 5. Impacts of pertussis toxin (PTX, $G\alpha_{o/i}$ inhibitor) and forskolin (FSK) on the number of Ki67⁺ cells in the presence or absence of THC or LPI. *GBM #4* and *GBM #10* were left untreated or

exposed to THC (a) or LPI (b) for 24 h, resulting in a decreased number of Ki67⁺ nuclei. A significantly decreased number of Ki67⁺ nuclei was detected after stimulation with PTX alone in GBM #4 and GBM #10. When THC (a) or LPI (b) were applied after PTX pre-incubation, neither inhibitory nor additive effects were observed. In GBM #4 and GBM #10, the number of Ki67⁺ nuclei was reduced concentration dependently after FSK stimulation for 24 h (c). FSK was applied in an ascending concentration series of 0.1 μM, 1 μM, 5 μM, 10 μM, and 30 μM. Significant effects were measured after incubation with ≥1 μM FSK. Data are means ± SEMs of N = 3 independent experiments performed in duplicate. Each red dot represents an individual data point. -/+ indicates without/with the corresponding substance. ++ denotes that cells were pre-incubated with PTX before THC or LPI was added. Significance was set at *p* < 0.05. The asterisk denotes significant results regarding the respective measurement indicated by the bar.

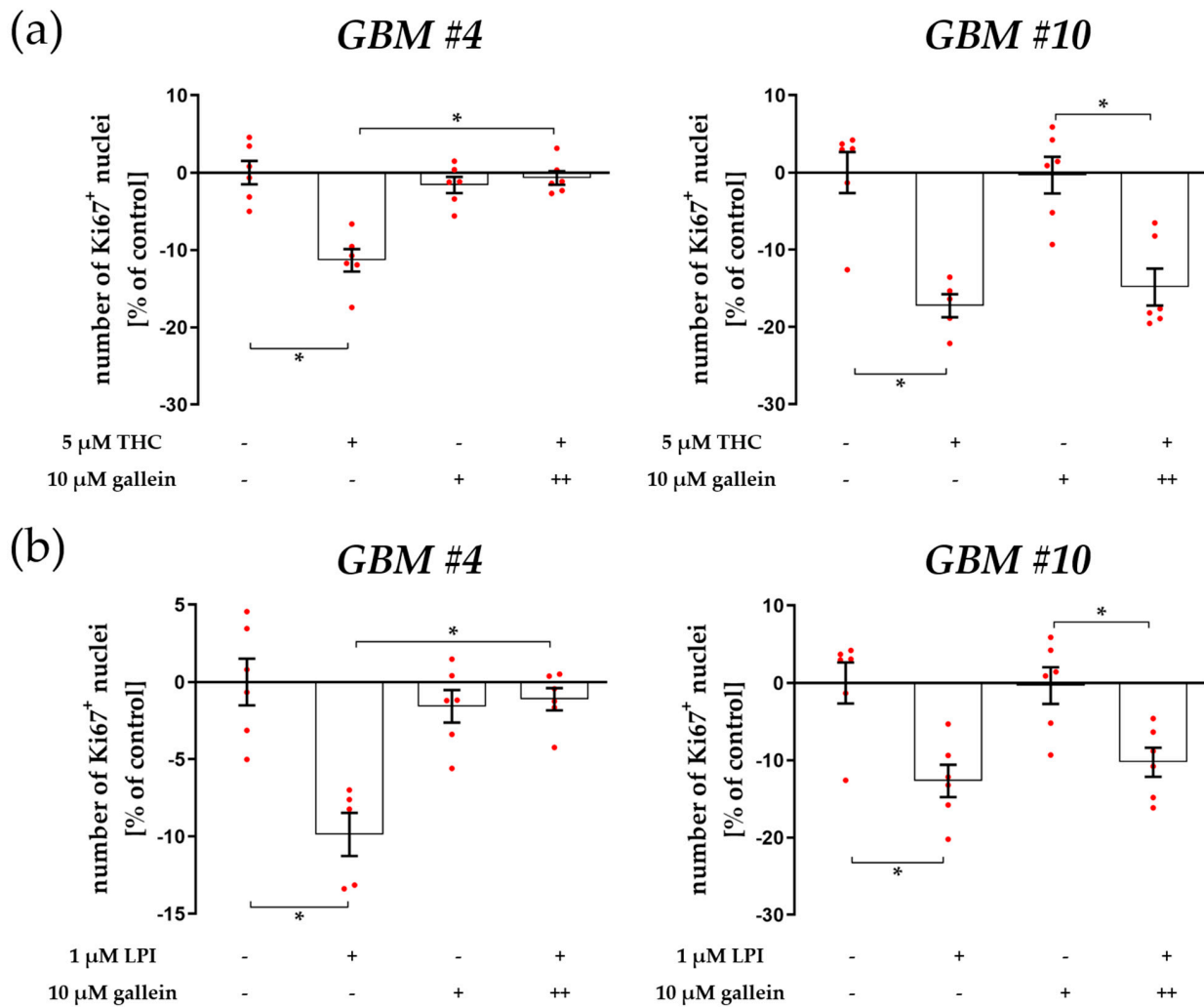


Figure 6. Impact of Gβγ inhibitor gallein on THC- and LPI-induced reduction of the number of Ki67⁺ nuclei. GBM #4 and GBM #10 were left untreated or exposed to THC (a) or LPI (b) for 24 h, resulting in a decreased number of Ki67⁺ nuclei. After cells were pre-incubated with gallein, responses to THC (a) and LPI (b) were significantly abolished in GBM #4. In contrast, in GBM #10, gallein caused no impact on THC- (a) and LPI-mediated signaling (b), reducing the number of Ki67⁺ nuclei. No alterations were observed when cells were stimulated with gallein alone (a,b). Data are means ± SEMs of N = 3 independent experiments performed in duplicate. Each red dot represents an individual data point. -/+ indicates without/with the corresponding substance. ++ denotes that cells were pre-incubated with gallein before THC or LPI was added. Significance was set at *p* < 0.05. The asterisk denotes significant results regarding the respective measurement indicated by the bar.

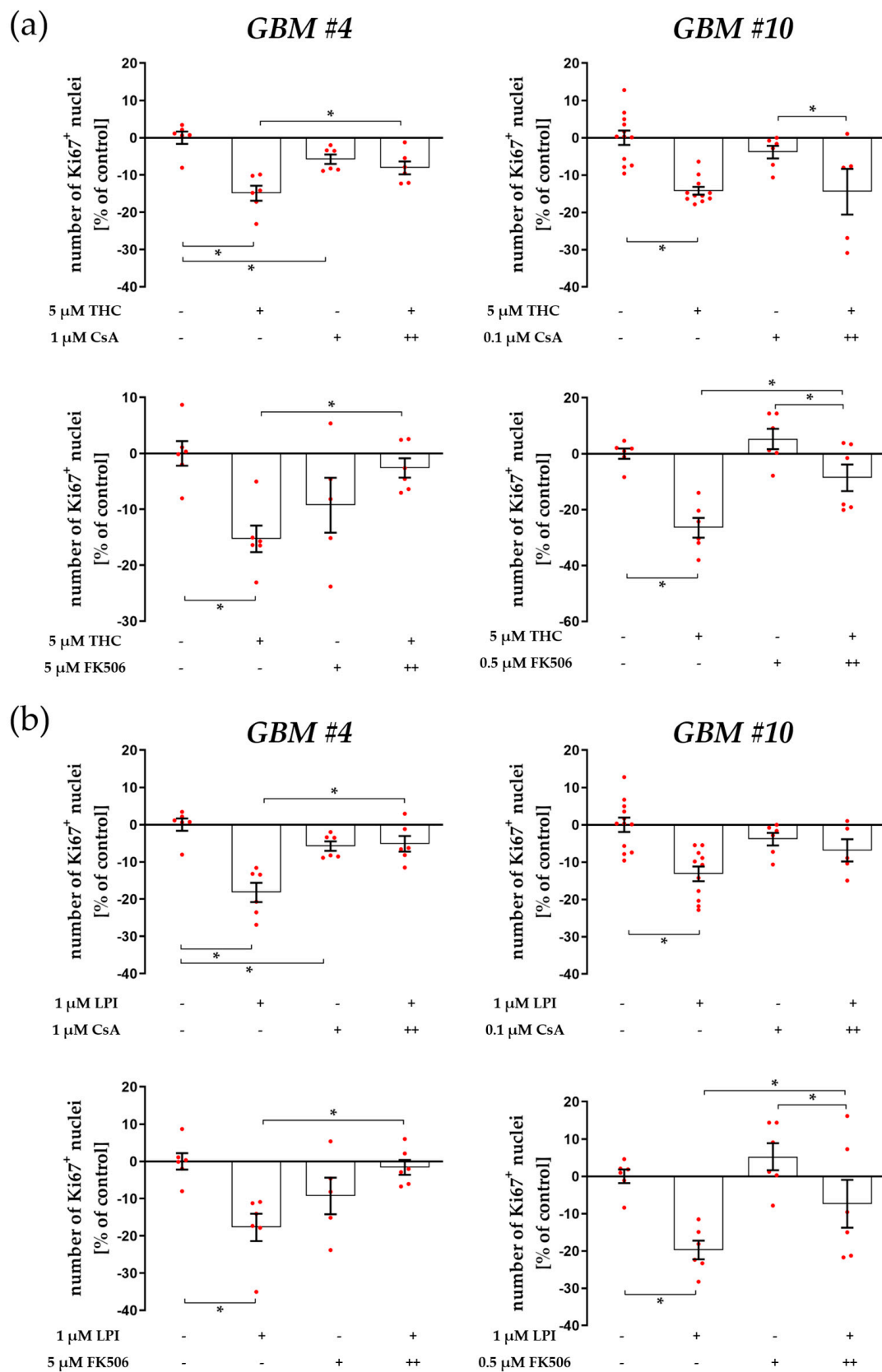


Figure 7. Impact of calcineurin inhibitor Cyclosporine A (CsA) and FK506 on THC- and LPI-induced reduction in the number of Ki67⁺ nuclei. GBM #4 and GBM #10 were left untreated or exposed to THC (a) or LPI (b) for 24 h, resulting in a decreased number of Ki67⁺ nuclei. In GBM #4, the effects of

THC (a) and LPI (b) were significantly reduced by CsA and FK506, but CsA alone elicited a decreased number of Ki67⁺ nuclei compared to the untreated control group. In *GBM #10*, lower concentrations of CsA and FK506 were used. No significant effects on responses to THC (a) and LPI (b) were observed in the presence of CsA, whereas FK506 partially inhibited the effects of THC (a) and LPI (b). Data are means \pm SEMs of N = 3 or N = 5 (*GBM #10*, CsA) independent experiments performed in duplicate. Each red dot represents an individual data point. -/+ indicates without/with the corresponding substance. ++ denotes that cells were pre-incubated with CsA or FK506 before THC or LPI was added. Significance was set at $p < 0.05$. The asterisk denotes significant results regarding the respective measurement indicated by the bar.

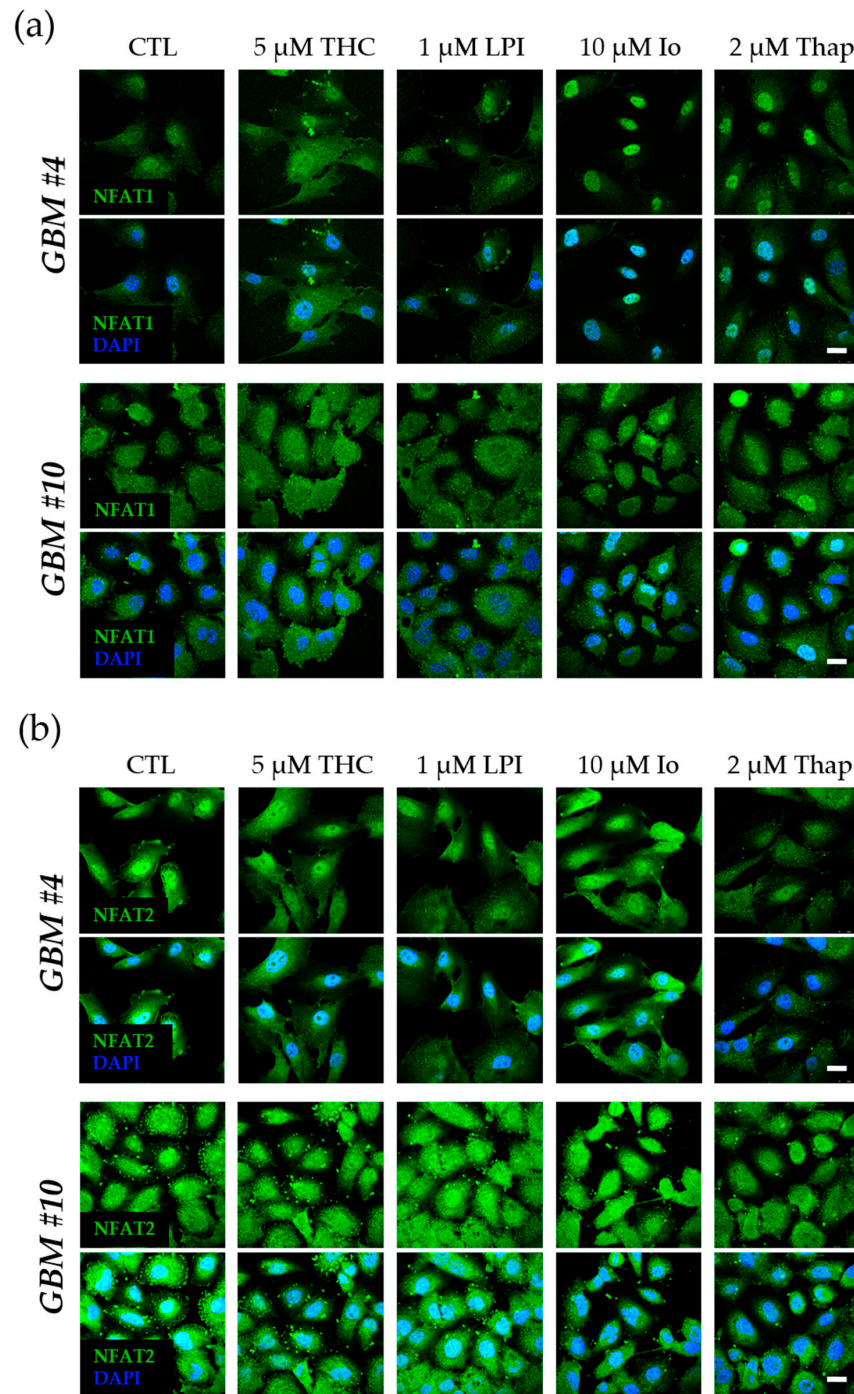


Figure 8. Influence of THC and LPI on the subcellular localization of NFAT1 and NFAT2 after 30 min. Representative images of NFAT1 (a) and NFAT2 (b) after 30 min of THC and LPI stimulation. In untreated

control cells, NFAT1 (a) and NFAT2 (b) were localized in both the cytoplasm and nucleus. Translocation of NFAT1 (a) and NFAT2 (b) after THC or LPI administration was not detectable in *GBM #4* or *GBM #10*. Increased signals of nuclear NFAT1 (a) were observed after ionomycin (Io) and thapsigargin (Thap) in both cell lines. In contrast, signals of NFAT2 (b) remained unchanged. Cell nuclei were counterstained with DAPI. Scale bar = 25 μ m.

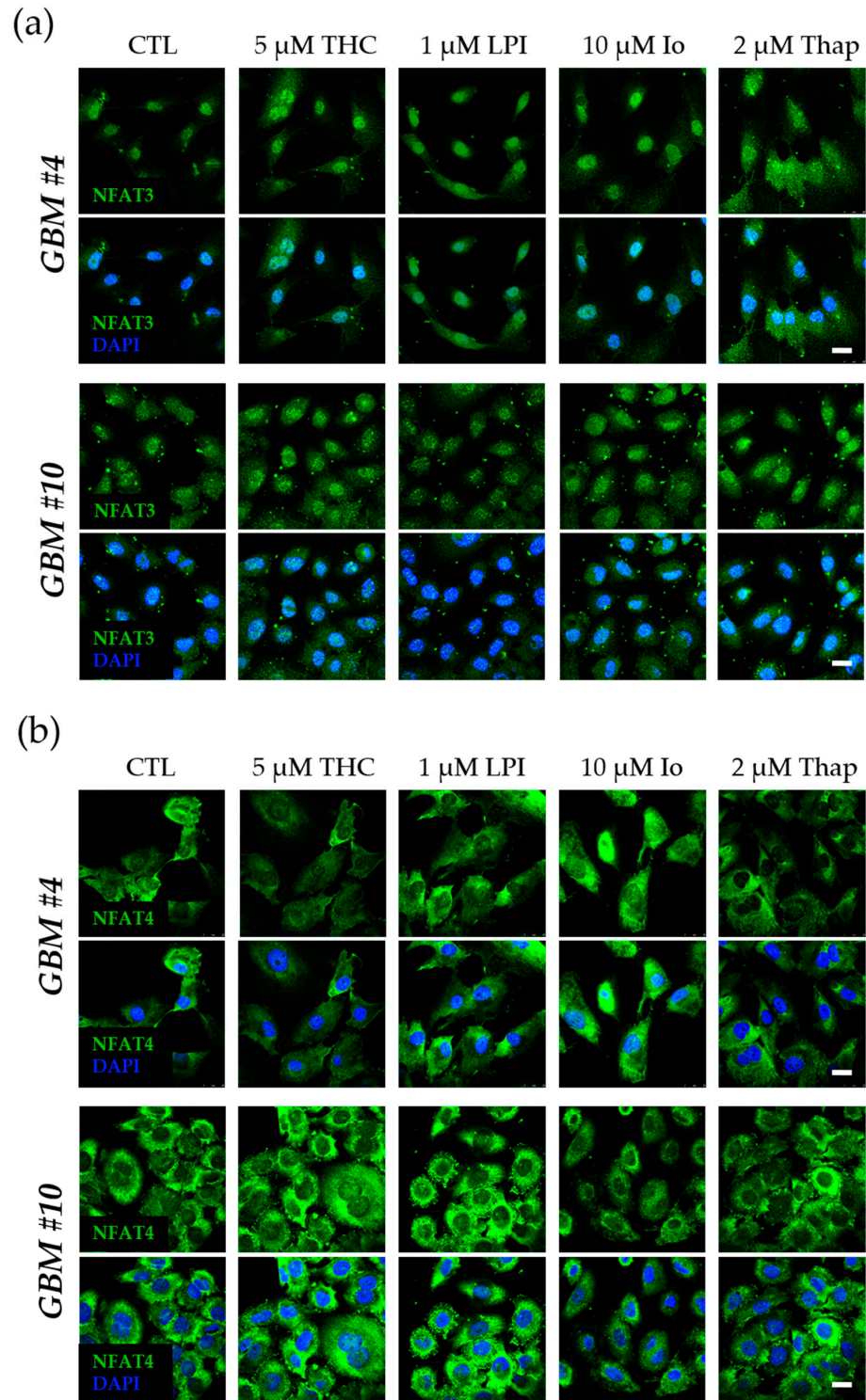


Figure 9. Influence of THC or LPI on the subcellular localization of NFAT3 and NFAT4 after 30 min. Representative images of NFAT3 (a) and NFAT4 (b) after 30 min of THC or LPI stimulation. In untreated control cells, NFAT3 (a) was mainly localized in the nucleus, and NFAT4 (b) was solely localized

in the cytoplasm. Translocation of NFAT3 (a) and NFAT4 (b) after THC, LPI, ionomycin (Io), and thapsigargin (Thap) administration was not detectable in *GBM #4* and *GBM #10*. Cell nuclei were counterstained with DAPI. Scale bar = 25 μm .

In contrast, ionomycin (Io, 10 μM) and thapsigargin (Thap, 2 μM), which both increased the intracellular calcium level via different mechanisms, led to an altered localization of NFAT1 after 30 min in *GBM #4* and *GBM #10*, reflected by higher nuclear signals of NFAT1 (Figures 8a and 10). Interestingly, localization of NFAT2, NFAT3, and NFAT4 remained unaffected by Io and Thap (Figures 8b and 9).

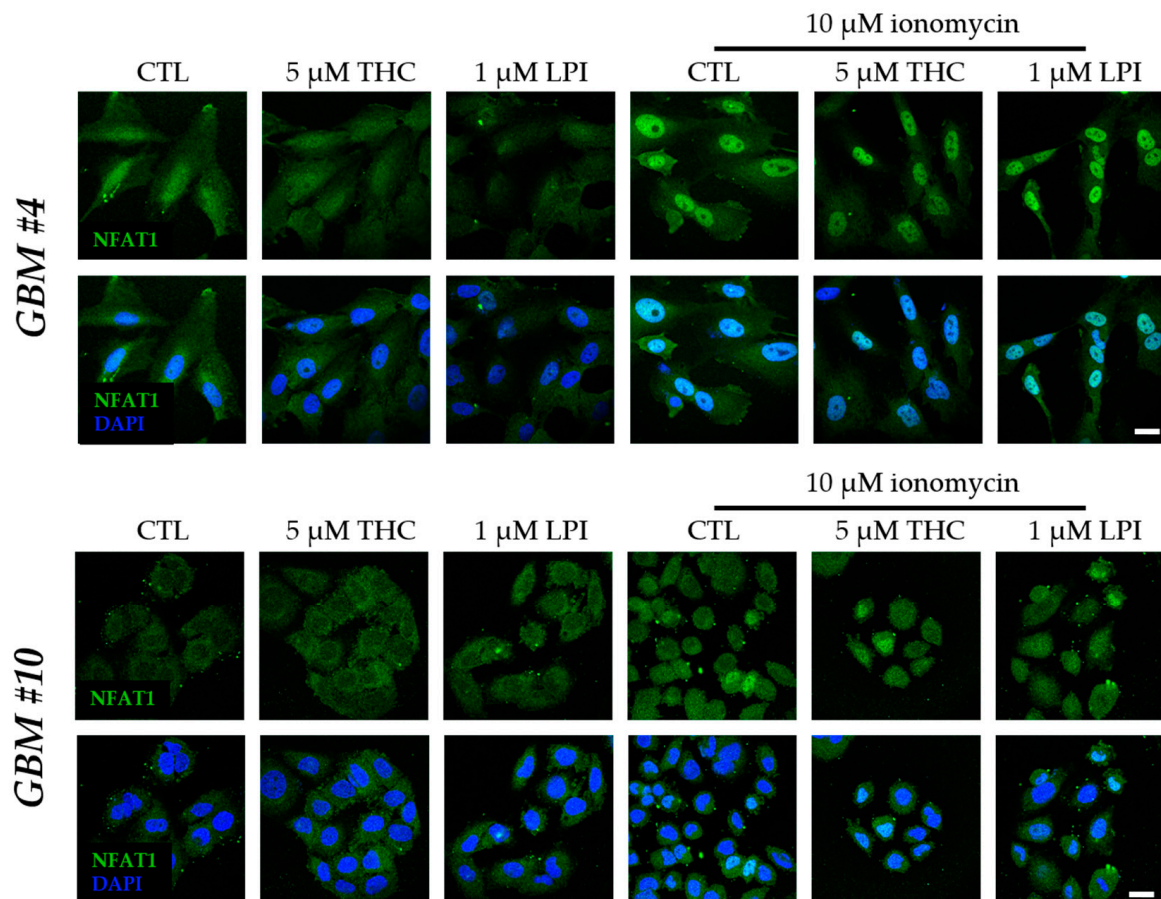


Figure 10. Influence of ionomycin on the subcellular localization of NFAT1 after 30 min in the presence of THC and LPI. THC and LPI had no effect on the subcellular localization of NFAT1 in *GBM #4* and *GBM #10*. Ionomycin (Io) induced a marked translocation of NFAT1 into the nucleus after 30 min. In the presence of THC or LPI, ionomycin's effects remained unchanged. Cell nuclei were counterstained with DAPI. Scale bar = 25 μm .

In addition, THC or LPI did not affect Io-induced translocation of NFAT1 into the nucleus (Figure 10). However, Io effects were fully blocked by calcineurin-inhibitors FK506 and CsA (Figure S9), indicating a calcineurin-dependent translocation of NFAT1 into the nucleus after Io treatment. Furthermore, the data confirm that the concentrations of FK506 and CsA used produced sufficient inhibition of calcineurin.

Remarkably, single stimulation with FK506 and CsA did not produce changes in nuclear signals of constitutively active NFAT2 and NFAT3 (Figure S10), suggesting calcineurin-independent activation of NFAT2 and NFAT3 or a low rate of NFAT nuclear exportation. Altogether, the data indicate an NFAT-independent regulation of the number of Ki67⁺ nuclei after THC or LPI treatment.

4. Discussion

The endocannabinoid system in general and cannabinoids in particular, like plant-derived THC and CBD, are believed to be promising targets and compounds for additional treatment strategies against highly malignant glioblastomas. They exert tumor-suppressive properties by inhibiting proliferation or inducing apoptosis, which are mostly mediated by cannabinoid-specific receptors such as CB₁ or CB₂ [14,18–20]. Based on their complex pharmacology, cannabinoids may also modulate cellular responses independently of classical CB₁/CB₂ receptors via other receptors such as GPR55 [2,22]. We recently discovered that THC affected the number of Ki67⁺ nuclei from patient-derived cells of human glioblastomas by GPR55 [16]. The focus of the present study was to characterize a part of the signaling pathway downstream of GPR55 that contributes an altered number of Ki67⁺ nuclei after THC or LPI treatment.

4.1. The Involvement of PLC-IP3 and RhoA-ROCK Signaling Pathways

GPR55 is thought to bind to Gα_{12/13} or Gα_q rather than Gα_s or Gα_{i/o} proteins [1,2,25]. Stimulation of Gα_q proteins is generally followed by an activation of PLC [2]. Studies on cell lines and primary cells of different origins revealed that pharmacological activation of GPR55 by LPI and other cannabinoids led to increased intracellular Ca²⁺ concentrations ([Ca²⁺]_i) via the activation of PLC and formation of IP3 [2,25,36,38]. In HEK293 cells and neurons of dorsal root ganglia, a PLC-IP3-dependent increase in [Ca²⁺]_i was observed after stimulation with 5 μM THC and 3 μM LPI [2]. The data of the present work indicate that the THC- and LPI-mediated reduction of Ki67⁺ nuclei might follow a PLC- and IP3-dependent mechanism via GPR55. PLC-IP3-dependent signal transductions through the activation of CB₁ and CB₂ receptors have so far not been reported for THC. In CB₁-transfected HEK293 cells, stimulation with 10 μM THC had no measurable effects on [Ca²⁺]_i, although CB₁-dependent Ca²⁺ release via WIN 55,212-2 was detected [39]. These results are highly consistent with CB₁/CB₂-independent effects of THC despite the presence of CB₁ receptors as reported previously [16] and support GPR55-specific signaling via PLC and IP3.

In addition, GPR55-mediated RhoA activation by LPI and cannabinoids was reported in HEK293 and PC12 cells [1,2,25,26,36]. RhoA-ROCK was shown to be activated downstream of Gα_{12/13} and to a lesser extent Gα_q. Since many cellular processes, such as proliferation or migration, might be regulated by RhoA and ROCK, the involvement of RhoA via the inhibition of ROCK was here investigated. A cell-type-specific RhoA-ROCK signaling was observed, indicating differences in intracellular coupling of G proteins to GPR55. Interestingly, in *GBM #10*, the reduction of the Ki67⁺ nuclei after THC and LPI stimulation might be explained by the interplay between PLC and RhoA-ROCK signaling pathways. In endothelial cells of a rat mesenteric arterial bed, an interaction between PLC- and RhoA-ROCK-modulated [Ca²⁺]_i was found after GPR55 activation by LPI or AM251 [36]. The release of intracellular Ca²⁺ was characterized by two phases. Inhibition of PLC by U73122 blocked the initial phase of Ca²⁺ release, whereas the late phase was abolished by inhibiting ROCK via Y-27632, suggesting a biphasic mechanism [36]. Both phases were abolished by blocking IP3-sensitive receptors with 2-APB, indicating ROCK-induced IP3 generation by direct PLC activation [36]. These data suggest a similar mechanism in *GBM #10* after THC or LPI stimulation, involving both PLC- and ROCK-dependent signaling.

The precise mechanism of ROCK-regulated PLC is not fully understood. In GPR55-expressing HEK293 cells, the actin cytoskeleton has been shown to play a pivotal role in the generation of GPR55-dependent Ca²⁺ signals. The family of Rho proteins, including RhoA, regulates protein biosynthesis and cell proliferation as well as the organization of the actin cytoskeleton by affecting actin stabilization through activation of LIM kinase or actomyosin contraction via MLC (modulator of VRAC current 1) [40]. RhoA activation and an intact actin cytoskeleton are required for the THC (5 μM) mediated rise in Ca²⁺ in HEK293 cells [2]. In contrast, pure PLC-mediated pathways as found upon the activation of muscarinic acetylcholine receptors of the parasympathetic nervous system were not affected

by either RhoA inhibition or deteriorated actin cytoskeleton formation [40]. Therefore, an intact actin cytoskeleton might play a central role in modulating $[Ca^{2+}]_i$ when GPR55 is coupled to RhoA-ROCK signaling. In murine fibroblast cell line NIH 3T3, a disrupted cytoskeleton altered the spatial interaction between PLC and IP₃-sensitive receptors, thus affecting PLC-dependent Ca^{2+} signaling [41]. Taken together, these data suggest that the RhoA-ROCK-signaling pathway may indirectly promote PLC-dependent reduction of Ki67⁺ nuclei in GBM #10 through alterations in the spatial location of PLC- and IP₃-sensitive receptors. The requirement for direct ROCK activation is supported by the ROCK-independent signaling in GBM #4, making the involvement of basal-active ROCK not evident.

4.2. Cell-Type-Dependent Coupling of GPR55 to $G\alpha_{12/13}$ and/or $G\alpha_q$ and the Role of $G\beta\gamma$

The divergence in RhoA-ROCK involvement suggests cell-type-specific differences in coupling to intracellular G proteins. Generally, RhoA-ROCK signaling is known to be activated downstream of $G\alpha_{12/13}$, whereas PLC activation is responsive to $G\alpha_q$ pathways [2]. Previous studies implicated intracellular coupling of GPR55 to $G\alpha_{12/13}$ and/or $G\alpha_q$ pathways [1,2,30]. Missing effects of the ROCK inhibitor in GBM #4 indicated a coupling of GPR55 signaling to $G\alpha_q$. In contrast, in GBM #10, GPR55-dependent signaling might be related to $G\alpha_{12/13}$ coupling or dual signaling via $G\alpha_q$ and $G\alpha_{12/13}$ due to PLC- and ROCK-dependent signaling. Comparable observations were conducted in GPR55-expressing HEK293 cells [25], in neurons of the dorsal root ganglia [2], and in mesenteric arterial endothelial cells [36], where a PLC- and RhoA-ROCK-dependent increase in $[Ca^{2+}]_i$ was measured. Moreover, increased $[Ca^{2+}]_i$ in the neurons of dorsal root ganglia after GPR55 activation was attributed to dual $G\alpha_{12/13}$ and $G\alpha_q$ signaling [2]. Some GPCRs functionally switch their associated subfamily of G proteins depending on the expression level of G proteins [39,42]. In the present work, differences in the expression of the relevant $G\alpha_q$ and $G\alpha_{12}$ subunits were found but did not explain cell-type-specific signaling.

GPCRs can initiate signaling cascades not only via $G\alpha$ subunits. Dissociation of the trimeric complexes after receptor activation also releases free and active $G\beta\gamma$ subunits that might be relevant for signal transduction events. Thus, the aspect of $G\beta\gamma$ -dependent signaling was further examined. A cell-type-specific $G\beta\gamma$ dependence was found. A correlation between $G\beta\gamma$ signaling and GPR55 has so far not been demonstrated in tumor cells. In murine slice cultures of the substantia nigra, GPR55 signaling induced by LPI or O-1602 was associated with the presynaptic release of [³H] gamma-amino-butyric acid (GABA) by a $G\beta\gamma$ -dependent mechanism [43]. In contrast to the present study, $G\beta\gamma$ -mediated AC activation with a subsequent cAMP accumulation was assumed to be an underlying mechanism [43], reflecting species- and cell-type-specific differences.

Although all isoforms of G proteins release one molecule of a $G\beta\gamma$ dimer per activation event, $G\beta\gamma$ signaling is strongly linked to $G\alpha_{i/o}$ -derived $G\beta\gamma$ subunits [44]. It is known that GPR55 does not interact with $G\alpha_{o/i}$ proteins. Alternatively, GPR55 is able to form heterodimers with $G\alpha_{o/i}$ -coupled receptors, as described for CB₁ [45], CB₂ [46,47], and LPA2 [48], resulting in an altered activity and signal transduction of GPR55. To test the involvement of $G\alpha_{o/i}$ proteins, PTX was used, as it prevents signal transduction of $G\alpha_{o/i}$ by catalyzing irreversible ADP-ribosylation of the α subunit of trimeric $G\alpha_{o/i}\beta\gamma$ complexes [49]. In our study, PTX was found to be unsuitable for analyzing $G\alpha_{o/i}$ -dependent signaling because it directly affected the number of Ki67⁺ nuclei. The responses to PTX could be explained by an accumulation of cAMP due to an enhanced cAMP production via stimulatory GPCRs and an unhindered activation of cAMP-mediated signaling pathways. As an alternative mechanism, $G\alpha_{o/i}$ -independent effects of PTX [50] should be considered, which occurred after using high concentrations of PTX. Direct stimulation of AC and cAMP production by FSK reduced the number of Ki67⁺ nuclei comparable to PTX, demonstrating unhindered activation of cAMP-mediated signaling pathways and confuting the $G\alpha_{o/i}$ -independent effects of PTX. As PTX treatment showed high background activity, the role of $G\alpha_{o/i}$ -derived $G\beta\gamma$ in GPR55 signaling in GBM #4 remains an open question.

G $\beta\gamma$ subunits are able to stimulate PLC directly or indirectly via PI3K [29,51–54]. Notably, G α_q -derived G $\beta\gamma$ subunits also have the capacity for signaling but to a lesser extent than those derived from G $\alpha_{i/o}$ and might generate signals via PI3K activation [55]. PI3K and PI3K-dependent PLC activation were described as mechanisms for GPR55-driven Ca²⁺ signaling in endothelial cells after AEA treatment [29]. Thus, in accordance with G α_q signaling in *GBM #4*, G α_q -derived G $\beta\gamma$ signaling via PI3K could be conceivable. Therefore, the involvement of PI3K should be investigated in further studies.

Alternatively, it was reported that G $\beta\gamma$ subunits might influence the extent of G α_q -dependent signaling through direct interaction with PLC [51,53,54]. On the one hand, G $\beta\gamma$ subunits were able to directly stimulate the activity of PLC [51,53] and thus act synergistically with the G α_q -dependent stimulation of PLC [52–54]. On the other hand, G $\beta\gamma$ subunits inhibit the G α -GTPase activity of PLC, as PLC is both an effector of G α_q and a G α_q -selective GTPase-activating protein (GAP) [53,56]. Since prevention of G $\beta\gamma$ disrupts interaction with their downstream effectors, it is conceivable that stimulation of PLC by G α_q alone was insufficient to exert effects after THC or LPI application. Therefore, in the case of *GBM #4*, a reduced number of Ki67⁺ nuclei by GPR55 might be determined by the duration and strength of PLC stimulation through interplay between G α_q and functional G $\beta\gamma$ subunits. The divergence of signaling observed in *GBM #10* might base on the coupling of GPR55, as *GBM #10* G $\alpha_{12/13}$ and ROCK activation directly or indirectly contributed to a sufficient duration and strength of PLC activation and/or downstream signals to modulate the number of Ki67⁺ nuclei. As discussed previously, this is in line with a biphasic increase in [Ca²⁺]_i by PLC and ROCK signaling in rat mesenteric arterial bed endothelial cells stimulated with LPI or AM251 [36]. It remains to be determined whether the functionality of GPR55, its G $\beta\gamma$, and RhoA-ROCK-dependent signaling and responsiveness to THC or LPI might be used as a positive prognostic marker.

4.3. Cell-Type-Specific Calcineurin Signaling and the Role of NFAT

Due to the involvement of IP₃-sensitive receptors, a Ca²⁺-dependent process was assumed in the present study [57]. Ca²⁺ functions as second messenger and activates various Ca²⁺-dependent protein kinases and calcineurin, a Ca²⁺/calmodulin-dependent protein phosphatase [58]. These enzymes act as transducers for transmitting Ca²⁺ signals from the cytosol to the nucleus. While Ca²⁺-dependent protein kinases activate transcription factors, including CREB or NF- κ B, by phosphorylation, calcineurin catalyzes dephosphorylation of the resident cytoplasmic transcription factor, such as NFAT [59]. Subsequently, NFAT translocates into the nucleus and induces or represses NFAT-specific genes. It is known that GPR55 is linked to an increased activity of NFAT via elevation of [Ca²⁺]_i [25,30]. To investigate the possibility of a calcineurin-dependent mechanism after THC and LPI treatment, we used two non-competitive calcineurin inhibitors (CsA and FK506), which limited the access of peptide and protein substrates to the active site of calcineurin [60,61]. Calcineurin-dependent signaling was observed in a cell-type-specific manner. Interestingly, partial inhibition of THC- and LPI-mediated effects in *GBM #10* after FK506 treatment was evident, whereas CsA had no detectable influence. This phenomenon might be explained by a higher binding affinity of FK506 complexes to calcineurin compared to CsA complexes [62].

However, no alterations in the subcellular localization of different isoforms of NFAT, namely NFAT1–4, were detected after THC or LPI stimulation. This is in strong contrast to calcineurin-dependent signaling in *GBM #4* but supports partial calcineurin-independent effects observed in *GBM #10*. The pronounced background activity of CsA and FK506 did not enable a clear conclusion and was unlikely to be attributable to the inhibition of basally active NFAT. After CsA and FK506 treatment, NFAT2 and NFAT3 were constitutively present in the nucleus, suggesting calcineurin-independent mechanisms in these tumor cells. Notably, the effects of both are not limited to calcineurin but also regulate the transcriptional activity of NF- κ B or proteasomal degradation [63].

The induction of NFAT in general and NFAT4 in particular was reported after LPI-driven GPR55 activation [25,29,64]. The differences compared to our study might be explained by the experimental conditions used, such as an artificial overexpression of GPR55 in HEK293 or serum starvation before and during stimulation experiments. Both conditions facilitate efficient NFAT activation by a prolonged Ca^{2+} stimulus due to increased responses resulting from the overstimulation of ectopic GPR55 expression and the absence of inhibitory components on Ca^{2+} signals that are present in the medium-containing serum. These conditions seemed to be absent in the glioblastoma cells investigated in this study. The intensity and duration of Ca^{2+} signals generated by store-operated calcium channels, such as IP3-sensitive receptors, play a crucial role in NFAT activation [59]. The activation of NFAT1 and NFAT4 required different strong and subcellular Ca^{2+} signals [65]. NFAT1 was selectively recruited at low stimulus intensities, whereas activation of both isoforms occurs with increasing receptor occupancy and continuous Ca^{2+} influx. Furthermore, different kinetics of the nuclear export of NFAT1 and NFAT4 were revealed. The slow export of NFAT1 allows activation of gene expression even in the presence of low-frequency Ca^{2+} spikes because NFAT1 remains in the nucleus longer after Ca^{2+} signals are terminated. In contrast, NFAT4 was only effective when Ca^{2+} mobilization was sustained, as its export was very rapid [65]. In the present study, we observed higher nuclear signals of NFAT1 after ionomycin or thapsigargin treatment, which both generated acute Ca^{2+} signaling [66,67]. In contrast, signals of NFAT2-4 remained unaffected. To obtain nuclear signals of NFAT2-4, co-treatment for inducing cooperation partners of NFAT such as c-Fos and c-Jun is likely needed. In NFAT overexpressing HEK293 cells, NFAT4-dependent luciferase expression was increased in response to ionomycin and PKC-activating PDBu but not to ionomycin alone [68]. Furthermore, NFAT4 showed pulsatile translocation dynamics, as found in mast cells [69].

However, in comparison to acute Ca^{2+} signals by ionomycin or thapsigargin, THC and LPI were unable to induce NFAT1 translocation. The requirement of a more prolonged Ca^{2+} stimulus to overcome glycogen synthase kinase 3 beta (GSK3 β) activity, which persistently phosphorylates NFAT and counteracts calcineurin dephosphorylating activity, might be a possible scenario for efficient NFAT1 activation.

Altogether, the data suggest that NFAT did not participate in the reduction of Ki67 after THC or LPI treatment. Furthermore, cell-type-specific calcineurin signaling gives rise to speculation that other calcineurin-dependent and calcineurin-independent signaling pathways are involved and react more sensitively to transient Ca^{2+} signals. Alternatively, basal NFAT activation, which was abrogated by FK506 and CsA, might be needed when it is acting as a coactivator for another transcription factor, which becomes active after THC and LPI treatment. However, in addition to NFAT, calcineurin also dephosphorylates other transcription factors, including CREB-regulated transcriptional coactivator (CRTC) 1 [70], transcription factor EB (TFEB) [71], myocyte enhancer factor 2 (MEF2) [72], and ETS Like-1 (ELK-1) [58]. Both CsA and FK506 might inhibit the transcriptional activity of NF- κ B, which may in turn become activated by Ca^{2+} /calmodulin-dependent protein kinase II (CaMKII). The mechanism behind the role of NF- κ B should further be explored as a calcineurin-independent mechanism.

Similar cell-type-dependent effects were observed in cAMP-mediated signaling pathways induced by PTX and FSK, which give rise to speculation of additional signaling pathways capable of reducing the number of Ki67⁺ nuclei. Here, the possible involvement of CREB should be highlighted. Although CREB is not a direct substrate for calcineurin, it might indirectly be regulated by calcineurin or by Ca^{2+} signals. For instance, calcineurin is a part of a negative feedback loop of Ca^{2+} -initiated transcription of CREB genes [73]. Interestingly, an increase in $[\text{Ca}^{2+}]_i$ activates CREB-directed gene transcription via activation of CaMKIV and subsequently induces inactivation of CREB via calcineurin-mediated activation of protein phosphatase-1 [73]. Alternatively, calcineurin can operate as a positive regulator of CREB by promoting nuclear translocation of CREB-regulated transcriptional co-activators (CRTCs) [70]. Under basal conditions, CRTCs retain their phosphorylated

form in the cytoplasm by interacting with 14-3-3 proteins. Both cAMP and Ca^{2+} signals can induce dephosphorylation of CRTCs by inhibition of salt-inducible kinases (SIKs, which phosphorylate CRTCs) or by the induction of calcineurin, respectively. Dephosphorylated CRTC translocates into the nucleus, binds to the bZIP domain of CREB, and operates as a co-activator [70]. The responsible underlying mechanism for an altered Ca^{2+} -dependent CREB activation is still not understood but might result from cell-type-specific differences and the amplitude, duration, and subcellular localization of Ca^{2+} signals [58]. These hypotheses should be considered in future investigations, including analyses of phosphorylation state, activity, and nuclear localization of CREB and CRTCs.

5. Conclusions

In the present work, signaling pathways related to GPR55 that might account for previously described THC-mediated reduction in the number of Ki67^+ nuclei of patient-derived glioblastoma cells were investigated. A strong involvement of the PLC-IP3 pathway was observed. Cell-type differences in $\text{G}\beta\gamma$ and RhoA-ROCK signaling were found, probably explained by differences in the coupling of GPR55 to intracellular G proteins. Additionally, GPR55-mediated effects required at least partial activation of calcineurin. Calcineurin-related activation of transcription factor NFAT was not evident after THC or LPI treatment, as its subcellular localization remained unchanged. However, the analysis of additional transcription factors, which are influenced by IP3-driven Ca^{2+} release and/or calcineurin, should be elucidated in future investigations to shed light on the precise mechanism of the GPR55-mediated reduction of Ki67^+ nuclei in glioblastoma cells. As the present study showed similarities and differences in GPR55-associated signaling compared to the literature, we may anticipate a better understanding of the complex pathways by which THC and GPR55 affect tumor cell biology in the context of glioblastomas. The data underline the diversity of GPR55-associated signaling pathways that are distinct in various cell types and from other cannabinoid receptors, including CB_1 and CB_2 .

Furthermore, this diversity might account in part for the individual responsiveness of tumor cells to GPR55 stimuli by cannabinoids. Nevertheless, the identification of the precise signaling pathway might be useful for the purpose of finding prognostic markers and defining the conditions in which THC and GPR55 may be beneficial or unemployable as novel therapeutic options.

Supplementary Materials: The following supporting information can be downloaded at: <https://www.mdpi.com/article/10.3390/cells12222646/s1>.

Author Contributions: Conceptualization, M.R.K., C.S. and F.D.; methodology, M.R.K., T.H., U.H., E.M. and J.I.; validation, M.R.K., J.P. and F.D.; formal analysis, M.R.K.; investigation, M.R.K., T.H. and U.H.; resources, J.P., J.I., C.S. and F.D.; data curation, M.R.K.; writing—original draft preparation, M.R.K.; writing—review and editing, M.R.K., T.H., U.H., E.M., R.G., J.P., J.I., C.S. and F.D.; visualization, M.R.K.; supervision, R.G., C.S. and F.D.; project administration, J.P. and F.D. All authors have read and agreed to the published version of the manuscript.

Funding: This research received no external funding.

Institutional Review Board Statement: The study was conducted in accordance with the Declaration of Helsinki and was approved by the local Ethics Committee of the University Halle-Wittenberg (project reference number: 2015-144).

Informed Consent Statement: Informed consent was obtained from all subjects involved in the study.

Data Availability Statement: Data are contained within the article and supplementary materials. The data of the current study has not been deposited in a public repository but is available from the lead author on request.

Acknowledgments: The authors would like to thank Chalid Ghadban, Candy Rothgänger-Strube, and Christin Zöller for their excellent technical assistance. We acknowledge the financial support from the funding program Open Access Publishing by the German Research Foundation (DFG).

Conflicts of Interest: The authors declare no conflict of interest.

References

1. Ryberg, E.; Larsson, N.; Sjögren, S.; Hjorth, S.; Hermansson, N.-O.; Leonova, J.; Elebring, T.; Nilsson, K.; Drmota, T.; Greasley, P.J. The Orphan Receptor GPR55 Is a Novel Cannabinoid Receptor: GPR55, a Novel Cannabinoid Receptor. *Br. J. Pharmacol.* **2009**, *152*, 1092–1101. [[CrossRef](#)] [[PubMed](#)]
2. Lauckner, J.E.; Jensen, J.B.; Chen, H.-Y.; Lu, H.-C.; Hille, B.; Mackie, K. GPR55 is a Cannabinoid Receptor that Increases Intracellular Calcium and Inhibits M Current. *Proc. Natl. Acad. Sci. USA* **2008**, *105*, 2699–2704. [[CrossRef](#)] [[PubMed](#)]
3. Sawzdargo, M.; Nguyen, T.; Lee, D.K.; Lynch, K.R.; Cheng, R.; Heng, H.H.Q.; George, S.R.; O'Dowd, B.F. Identification and Cloning of Three Novel Human G Protein-Coupled Receptor Genes GPR52, Ψ GPR53 and GPR55: GPR55 is Extensively Expressed in Human Brain. *Mol. Brain Res.* **1999**, *64*, 193–198. [[CrossRef](#)] [[PubMed](#)]
4. Staton, P.C.; Hatcher, J.P.; Walker, D.J.; Morrison, A.D.; Shapland, E.M.; Hughes, J.P.; Chong, E.; Mander, P.K.; Green, P.J.; Billinton, A.; et al. The Putative Cannabinoid Receptor GPR55 Plays a Role in Mechanical Hyperalgesia Associated with Inflammatory and Neuropathic Pain. *Pain* **2008**, *139*, 225–236. [[CrossRef](#)]
5. Pietr, M.; Kozela, E.; Levy, R.; Rimmerman, N.; Lin, Y.H.; Stella, N.; Vogel, Z.; Juknat, A. Differential Changes in GPR55 during Microglial Cell Activation. *FEBS Lett.* **2009**, *583*, 2071–2076. [[CrossRef](#)]
6. Henstridge, C.M.; Balenga, N.A.B.; Kargl, J.; Andradas, C.; Brown, A.J.; Irving, A.; Sanchez, C.; Waldhoer, M. Minireview: Recent Developments in the Physiology and Pathology of the Lysophosphatidylinositol-Sensitive Receptor GPR55. *Mol. Endocrinol.* **2011**, *25*, 1835–1848. [[CrossRef](#)]
7. Oka, S.; Kimura, S.; Toshida, T.; Ota, R.; Yamashita, A.; Sugiura, T. Lysophosphatidylinositol Induces Rapid Phosphorylation of P38 Mitogen-Activated Protein Kinase and Activating Transcription Factor 2 in HEK293 Cells Expressing GPR55 and IM-9 Lymphoblastoid Cells. *J. Biochem.* **2010**, *147*, 671–678. [[CrossRef](#)]
8. Kremshofer, J.; Siwetz, M.; Berghold, V.M.; Lang, I.; Huppertz, B.; Gauster, M. A Role for GPR55 in Human Placental Venous Endothelial Cells. *Histochem. Cell Biol.* **2015**, *144*, 49–58. [[CrossRef](#)]
9. Simcocks, A.C.; O'Keefe, L.; Jenkin, K.A.; Mathai, M.L.; Hryciw, D.H.; McAinch, A.J. A Potential Role for GPR55 in the Regulation of Energy Homeostasis. *Drug Discov. Today* **2014**, *19*, 1145–1151. [[CrossRef](#)]
10. Andradas, C.; Caffarel, M.M.; Pérez-Gómez, E.; Salazar, M.; Lorente, M.; Velasco, G.; Guzmán, M.; Sánchez, C. The Orphan G Protein-Coupled Receptor GPR55 Promotes Cancer Cell Proliferation via ERK. *Oncogene* **2011**, *30*, 245–252. [[CrossRef](#)]
11. Kargl, J.; Andersen, L.; Hasenöhr, C.; Feuersinger, D.; Stančić, A.; Fauland, A.; Magnes, C.; El-Heliebi, A.; Lax, S.; Uranitsch, S.; et al. GPR55 Promotes Migration and Adhesion of Colon Cancer Cells Indicating a Role in Metastasis: GPR55 in Colon Cancer. *Br. J. Pharmacol.* **2016**, *173*, 142–154. [[CrossRef](#)] [[PubMed](#)]
12. Ferro, R.; Adamska, A.; Lattanzio, R.; Mavrommati, I.; Edling, C.E.; Arifin, S.A.; Fyffe, C.A.; Sala, G.; Sacchetto, L.; Chiorino, G.; et al. GPR55 Signalling Promotes Proliferation of Pancreatic Cancer Cells and Tumour Growth in Mice, and Its Inhibition Increases Effects of Gemcitabine. *Oncogene* **2018**, *37*, 6368–6382. [[CrossRef](#)] [[PubMed](#)]
13. Hohmann, T.; Grabiec, U.; Ghadban, C.; Feese, K.; Dehghani, F. The Influence of Biomechanical Properties and Cannabinoids on Tumor Invasion. *Cell Adh. Migr.* **2017**, *11*, 54–67. [[CrossRef](#)] [[PubMed](#)]
14. Hohmann, T.; Feese, K.; Greither, T.; Ghadban, C.; Jäger, V.; Dehghani, F.; Grabiec, U. Synthetic Cannabinoids Influence the Invasion of Glioblastoma Cell Lines in a Cell- and Receptor-Dependent Manner. *Cancers* **2019**, *11*, 161. [[CrossRef](#)] [[PubMed](#)]
15. Hohmann, T.; Feese, K.; Ghadban, C.; Dehghani, F.; Grabiec, U. On the Influence of Cannabinoids on Cell Morphology and Motility of Glioblastoma Cells. *PLoS ONE* **2019**, *14*, e0212037. [[CrossRef](#)]
16. Kolbe, M.R.; Hohmann, T.; Hohmann, U.; Ghadban, C.; Mackie, K.; Zöller, C.; Prell, J.; Illert, J.; Strauss, C.; Dehghani, F. THC Reduces Ki67-Immunoreactive Cells Derived from Human Primary Glioblastoma in a GPR55-Dependent Manner. *Cancers* **2021**, *13*, 1064. [[CrossRef](#)]
17. Zhang, X.; Qin, Y.; Pan, Z.; Li, M.; Liu, X.; Chen, X.; Qu, G.; Zhou, L.; Xu, M.; Zheng, Q.; et al. Cannabidiol Induces Cell Cycle Arrest and Cell Apoptosis in Human Gastric Cancer SGC-7901 Cells. *Biomolecules* **2019**, *9*, 302. [[CrossRef](#)] [[PubMed](#)]
18. Galanti, G.; Fisher, T.; Kventsel, I.; Shoham, J.; Gallily, R.; Mechoulam, R.; Lavie, G.; Amariglio, N.; Rechavi, G.; Toren, A. Δ^9 -Tetrahydrocannabinol Inhibits Cell Cycle Progression by Downregulation of E2F1 in Human Glioblastoma Multiforme Cells. *Acta Oncol.* **2008**, *47*, 1062–1070. [[CrossRef](#)]
19. Caffarel, M.M.; Sarrió, D.; Palacios, J.; Guzmán, M.; Sánchez, C. Δ^9 -Tetrahydrocannabinol Inhibits Cell Cycle Progression in Human Breast Cancer Cells through Cdc2 Regulation. *Cancer Res.* **2006**, *66*, 6615–6621. [[CrossRef](#)]
20. Sánchez, C.; Galve-Roperh, I.; Canova, C.; Brachet, P.; Guzmán, M. Delta9-Tetrahydrocannabinol Induces Apoptosis in C6 Glioma Cells. *FEBS Lett.* **1998**, *436*, 6–10. [[CrossRef](#)]
21. Carracedo, A.; Lorente, M.; Egia, A.; Blázquez, C.; García, S.; Giroux, V.; Malicet, C.; Villuendas, R.; Gironella, M.; González-Feria, L.; et al. The Stress-Regulated Protein P8 Mediates Cannabinoid-Induced Apoptosis of Tumor Cells. *Cancer Cell* **2006**, *9*, 301–312. [[CrossRef](#)] [[PubMed](#)]
22. Morales, P.; Hurst, D.P.; Reggio, P.H. Molecular Targets of the Phytocannabinoids: A Complex Picture. In *Phytocannabinoids*; Kinghorn, A.D., Falk, H., Gibbons, S., Kobayashi, J., Eds.; Springer International Publishing: Cham, Switzerland, 2017; Volume 103, pp. 103–131. ISBN 978-3-319-45539-6.

23. Huang, L.; Ramirez, J.C.; Frampton, G.A.; Golden, L.E.; Quinn, M.A.; Pae, H.Y.; Horvat, D.; Liang, L.; DeMorrow, S. Anandamide Exerts Its Antiproliferative Actions on Cholangiocarcinoma by Activation of the GPR55 Receptor. *Lab. Investig.* **2011**, *91*, 1007–1017. [[CrossRef](#)] [[PubMed](#)]
24. Akimov, M.G.; Gretskeya, N.M.; Dudina, P.V.; Sherstyanykh, G.D.; Zinchenko, G.N.; Serova, O.V.; Degtyaryova, K.O.; Deyev, I.E.; Bezuglov, V.V. The Mechanisms of GPR55 Receptor Functional Selectivity during Apoptosis and Proliferation Regulation in Cancer Cells. *Int. J. Mol. Sci.* **2023**, *24*, 5524. [[CrossRef](#)] [[PubMed](#)]
25. Henstridge, C.M.; Balenga, N.A.B.; Ford, L.A.; Ross, R.A.; Waldhoer, M.; Irving, A.J. The GPR55 Ligand L- α -lysophosphatidylinositol Promotes RhoA-dependent Ca²⁺ Signaling and NFAT Activation. *FASEB J.* **2009**, *23*, 183–193. [[CrossRef](#)] [[PubMed](#)]
26. Obara, Y.; Ueno, S.; Yanagihata, Y.; Nakahata, N. Lysophosphatidylinositol Causes Neurite Retraction via GPR55, G13 and RhoA in PC12 Cells. *PLoS ONE* **2011**, *6*, e24284. [[CrossRef](#)]
27. Piñeiro, R.; Maffucci, T.; Falasca, M. The Putative Cannabinoid Receptor GPR55 Defines a Novel Autocrine Loop in Cancer Cell Proliferation. *Oncogene* **2011**, *30*, 142–152. [[CrossRef](#)]
28. Vong, C.T.; Tseng, H.H.L.; Kwan, Y.W.; Lee, S.M.-Y.; Hoi, M.P.M. G-Protein Coupled Receptor 55 Agonists Increase Insulin Secretion through Inositol Trisphosphate-Mediated Calcium Release in Pancreatic β -Cells. *Eur. J. Pharmacol.* **2019**, *854*, 372–379. [[CrossRef](#)]
29. Waldeck-Weiermair, M.; Zoratti, C.; Osibow, K.; Balenga, N.; Goessnitzer, E.; Waldhoer, M.; Malli, R.; Graier, W.F. Integrin Clustering Enables Anandamide-Induced Ca²⁺ Signaling in Endothelial Cells via GPR55 by Protection against CB1-Receptor-Triggered Repression. *J. Cell Sci.* **2008**, *121*, 1704–1717. [[CrossRef](#)]
30. Henstridge, C.M.; Balenga, N.A.; Schröder, R.; Kargl, J.K.; Platzer, W.; Martini, L.; Arthur, S.; Penman, J.; Whistler, J.L.; Kostenis, E.; et al. GPR55 Ligands Promote Receptor Coupling to Multiple Signalling Pathways: GPR55 Signalling. *Br. J. Pharmacol.* **2010**, *160*, 604–614. [[CrossRef](#)]
31. Shen, X.; Jiang, H.; Ying, M.; Xie, Z.; Li, X.; Wang, H.; Zhao, J.; Lin, C.; Wang, Y.; Feng, S.; et al. Calcineurin Inhibitors Cyclosporin A and Tacrolimus Protect against Podocyte Injury Induced by Puromycin Aminonucleoside in Rodent Models. *Sci. Rep.* **2016**, *6*, 32087. [[CrossRef](#)]
32. Maguire, O.; Tornatore, K.M.; O’Loughlin, K.L.; Venuto, R.C.; Minderman, H. Nuclear Translocation of Nuclear Factor of Activated T Cells (NFAT) as a Quantitative Pharmacodynamic Parameter for Tacrolimus. *Cytom. Part A* **2013**, *83*, 1096–1104. [[CrossRef](#)] [[PubMed](#)]
33. Surve, C.R.; Lehmann, D.; Smrcka, A.V. A Chemical Biology Approach Demonstrates G Protein By Subunits Are Sufficient to Mediate Directional Neutrophil Chemotaxis. *J. Biol. Chem.* **2014**, *289*, 17791–17801. [[CrossRef](#)] [[PubMed](#)]
34. Oka, S.; Nakajima, K.; Yamashita, A.; Kishimoto, S.; Sugiura, T. Identification of GPR55 as a Lysophosphatidylinositol Receptor. *Biochem. Biophys. Res. Commun.* **2007**, *362*, 928–934. [[CrossRef](#)] [[PubMed](#)]
35. Small-Howard, A.L.; Shimoda, L.M.N.; Adra, C.N.; Turner, H. Anti-Inflammatory Potential of CB1-Mediated cAMP Elevation in Mast Cells. *Biochem. J.* **2005**, *388*, 465–473. [[CrossRef](#)] [[PubMed](#)]
36. AlSuleimani, Y.M.; Hiley, C.R. The GPR55 Agonist Lysophosphatidylinositol Relaxes Rat Mesenteric Resistance Artery and Induces Ca²⁺ Release in Rat Mesenteric Artery Endothelial Cells: The GPR55 Agonist Lysophosphatidylinositol. *Br. J. Pharmacol.* **2015**, *172*, 3043–3057. [[CrossRef](#)] [[PubMed](#)]
37. Nakajima, K.; Oka, S.; Tanikawa, T.; Nemoto-Sasaki, Y.; Matsumoto, N.; Ishiguro, H.; Arata, Y.; Sugiura, T.; Yamashita, A. Lysophosphatidylinositol Induced Morphological Changes and Stress Fiber Formation through the GPR55-RhoA-ROCK Pathway. *Int. J. Mol. Sci.* **2022**, *23*, 10932. [[CrossRef](#)]
38. Akimov, M.G.; Gamisonia, A.M.; Dudina, P.V.; Gretskeya, N.M.; Gaydaryova, A.A.; Kuznetsov, A.S.; Zinchenko, G.N.; Bezuglov, V.V. GPR55 Receptor Activation by the N-Acyl Dopamine Family Lipids Induces Apoptosis in Cancer Cells via the Nitric Oxide Synthase (nNOS) Over-Stimulation. *Int. J. Mol. Sci.* **2021**, *22*, 622. [[CrossRef](#)]
39. Lauckner, J.E.; Hille, B.; Mackie, K. The Cannabinoid Agonist WIN55,212-2 Increases Intracellular Calcium via CB1 Receptor Coupling to Gq/11 G Proteins. *Proc. Natl. Acad. Sci. USA* **2005**, *102*, 19144–19149. [[CrossRef](#)]
40. Marzban, H.; Kong, J.; Mehr, S.; Vriend, J.; Li, J.; Guan, T.; Chung, S.; Mirzaei, N.; Marzban, A.; Shojaei, S.; et al. Mevalonate Cascade and Neurodevelopmental and Neurodegenerative Diseases: Future Targets for Therapeutic Application. *Curr. Mol. Pharmacol.* **2017**, *10*, 115–140. [[CrossRef](#)]
41. Ribeiro, C.M.P.; Reece, J.; Putney, J.W. Role of the Cytoskeleton in Calcium Signaling in NIH 3T3 Cells. *J. Biol. Chem.* **1997**, *272*, 26555–26561. [[CrossRef](#)]
42. Finlay, D.B.; Cawston, E.E.; Grimsey, N.L.; Hunter, M.R.; Korde, A.; Vemuri, V.K.; Makriyannis, A.; Glass, M. G α_s Signalling of the CB₁ Receptor and the Influence of Receptor Number: CB₁ Receptor G α_s Signalling. *Br. J. Pharmacol.* **2017**, *174*, 2545–2562. [[CrossRef](#)] [[PubMed](#)]
43. Sánchez-Zavaleta, R.; Ávalos-Fuentes, J.A.; González-Hernández, A.V.; Recillas-Morales, S.; Paz-Bermúdez, F.J.; Leyva-Gómez, G.; Cortés, H.; Florán, B. Presynaptic Nigral GPR55 Receptors Stimulate [³H]-GABA Release through [³H]-cAMP Production and PKA Activation and Promote Motor Behavior. *Synapse* **2022**, *76*, e22246. [[CrossRef](#)] [[PubMed](#)]
44. Pfeil, E.M.; Brands, J.; Merten, N.; Vögtle, T.; Vescovo, M.; Rick, U.; Albrecht, I.-M.; Heycke, N.; Kawakami, K.; Ono, Y.; et al. Heterotrimeric G Protein Subunit G α_q Is a Master Switch for G $\beta\gamma$ -Mediated Calcium Mobilization by Gi-Coupled GPCRs. *Mol. Cell* **2020**, *80*, 940–954.e6. [[CrossRef](#)] [[PubMed](#)]

45. Kargl, J.; Balenga, N.; Parzmair, G.P.; Brown, A.J.; Heinemann, A.; Waldhoer, M. The Cannabinoid Receptor CB1 Modulates the Signaling Properties of the Lysophosphatidylinositol Receptor GPR55. *J. Biol. Chem.* **2012**, *287*, 44234–44248. [[CrossRef](#)] [[PubMed](#)]
46. Moreno, E.; Andradas, C.; Medrano, M.; Caffarel, M.M.; Pérez-Gómez, E.; Blasco-Benito, S.; Gómez-Cañas, M.; Pazos, M.R.; Irving, A.J.; Lluís, C.; et al. Targeting CB₂-GPR55 Receptor Heteromers Modulates Cancer Cell Signaling. *J. Biol. Chem.* **2014**, *289*, 21960–21972. [[CrossRef](#)]
47. Balenga, N.A.; Martínez-Pinilla, E.; Kargl, J.; Schröder, R.; Peinhaupt, M.; Platzter, W.; Bálint, Z.; Zamarbide, M.; Dopeso-Reyes, I.G.; Ricobaraza, A.; et al. Heteromerization of GPR55 and Cannabinoid CB₂ Receptors Modulates Signalling: Heteromerization of GPR55 and CB₂ Receptors. *Br. J. Pharmacol.* **2014**, *171*, 5387–5406. [[CrossRef](#)] [[PubMed](#)]
48. Bang, G.; Ghil, S. BRET Analysis Reveals Interaction between the Lysophosphatidic Acid Receptor LPA2 and the Lysophosphatidylinositol Receptor GPR55 in Live Cells. *FEBS Lett.* **2021**, *595*, 1806–1818. [[CrossRef](#)] [[PubMed](#)]
49. Mangmool, S.; Kurose, H. Gi/o Protein-Dependent and -Independent Actions of Pertussis Toxin (PTX). *Toxins* **2011**, *3*, 884–899. [[CrossRef](#)]
50. Nishida, M.; Suda, R.; Nagamatsu, Y.; Tanabe, S.; Onohara, N.; Nakaya, M.; Kanaho, Y.; Shibata, T.; Uchida, K.; Sumimoto, H.; et al. Pertussis Toxin Up-Regulates Angiotensin Type 1 Receptors through Toll-like Receptor 4-Mediated Rac Activation. *J. Biol. Chem.* **2010**, *285*, 15268–15277. [[CrossRef](#)]
51. Smrcka, A.V.; Sternweis, P.C. Regulation of Purified Subtypes of Phosphatidylinositol-Specific Phospholipase C Beta by G Protein Alpha and Beta Gamma Subunits. *J. Biol. Chem.* **1993**, *268*, 9667–9674. [[CrossRef](#)]
52. Philip, F.; Kadamur, G.; Silos, R.G.; Woodson, J.; Ross, E.M. Synergistic Activation of Phospholipase C-B3 by Gαq and Gβγ Describes a Simple Two-State Coincidence Detector. *Curr. Biol.* **2010**, *20*, 1327–1335. [[CrossRef](#)] [[PubMed](#)]
53. Litosch, I. RhoA Co-Ordinates with Heterotrimeric G Proteins to Regulate Efficacy. *Biochem. Biophys. Res. Commun.* **2011**, *415*, 215–219. [[CrossRef](#)] [[PubMed](#)]
54. Rebres, R.A.; Roach, T.I.A.; Fraser, I.D.C.; Philip, F.; Moon, C.; Lin, K.-M.; Liu, J.; Santat, L.; Cheadle, L.; Ross, E.M.; et al. Synergistic Ca²⁺ Responses by Gαi- and Gαq-Coupled G-Protein-Coupled Receptors Require a Single PLCβ Isoform That is Sensitive to Both Gβγ and Gαq. *J. Biol. Chem.* **2011**, *286*, 942–951. [[CrossRef](#)] [[PubMed](#)]
55. White, A.D.; Jean-Alphonse, F.G.; Fang, F.; Peña, K.A.; Liu, S.; König, G.M.; Inoue, A.; Aslanoglou, D.; Gellman, S.H.; Kostenis, E.; et al. G_{q/11}-Dependent Regulation of Endosomal cAMP Generation by Parathyroid Hormone Class B GPCR. *Proc. Natl. Acad. Sci. USA* **2020**, *117*, 7455–7460. [[CrossRef](#)]
56. Tang, W.; Tu, Y.; Nayak, S.K.; Woodson, J.; Jehl, M.; Ross, E.M. Gβγ Inhibits Gα GTPase-Activating Proteins by Inhibition of Gα-GTP Binding during Stimulation by Receptor. *J. Biol. Chem.* **2006**, *281*, 4746–4753. [[CrossRef](#)]
57. Prole, D.L.; Taylor, C.W. Structure and Function of IP₃ Receptors. *Cold Spring Harb. Perspect. Biol.* **2019**, *11*, a035063. [[CrossRef](#)]
58. Thiel, G.; Schmidt, T.; Rössler, O.G. Ca²⁺ Microdomains, Calcineurin and the Regulation of Gene Transcription. *Cells* **2021**, *10*, 875. [[CrossRef](#)]
59. Park, Y.-J.; Yoo, S.-A.; Kim, M.; Kim, W.-U. The Role of Calcium–Calcineurin–NFAT Signaling Pathway in Health and Autoimmune Diseases. *Front. Immunol.* **2020**, *11*, 195. [[CrossRef](#)]
60. Kissinger, C.R.; Parge, H.E.; Knighton, D.R.; Lewis, C.T.; Pelletier, L.A.; Tempczyk, A.; Kalish, V.J.; Tucker, K.D.; Showalter, R.E.; Moomaw, E.W.; et al. Crystal Structures of Human Calcineurin and the Human FKBP12–FK506–Calcineurin Complex. *Nature* **1995**, *378*, 641–644. [[CrossRef](#)]
61. Jin, L.; Harrison, S.C. Crystal Structure of Human Calcineurin Complexed with Cyclosporin A and Human Cyclophilin. *Proc. Natl. Acad. Sci. USA* **2002**, *99*, 13522–13526. [[CrossRef](#)]
62. Fruman, D.A.; Klee, C.B.; Biederer, B.E.; Burakoff, S.J. Calcineurin Phosphatase Activity in T Lymphocytes is Inhibited by FK 506 and Cyclosporin A. *Proc. Natl. Acad. Sci. USA* **1992**, *89*, 3686–3690. [[CrossRef](#)] [[PubMed](#)]
63. Meyer, S.; Kohler, N.G.; Joly, A. Cyclosporine A Is an Uncompetitive Inhibitor of Proteasome Activity and Prevents NF-κB Activation. *FEBS Lett.* **1997**, *413*, 354–358. [[CrossRef](#)] [[PubMed](#)]
64. Kargl, J.; Brown, A.J.; Andersen, L.; Dorn, G.; Schicho, R.; Waldhoer, M.; Heinemann, A. A Selective Antagonist Reveals a Potential Role of G Protein–Coupled Receptor 55 in Platelet and Endothelial Cell Function. *J. Pharmacol. Exp. Ther.* **2013**, *346*, 54–66. [[CrossRef](#)] [[PubMed](#)]
65. Kar, P.; Parekh, A.B. Distinct Spatial Ca²⁺ Signatures Selectively Activate Different NFAT Transcription Factor Isoforms. *Mol. Cell* **2015**, *58*, 232–243. [[CrossRef](#)]
66. Morgan, A.J.; Jacob, R. Ionomycin Enhances Ca²⁺ Influx by Stimulating Store-Regulated Cation Entry and Not by a Direct Action at the Plasma Membrane. *Biochem. J.* **1994**, *300*, 665–672. [[CrossRef](#)]
67. Razani-Boroujerdi, S.; Partridge, L.D.; Sopori, M.L. Intracellular Calcium Signaling Induced by Thapsigargin in Excitable and Inexcitable Cells. *Cell Calcium* **1994**, *16*, 467–474. [[CrossRef](#)]
68. Vihma, H.; Luhakooder, M.; Pruunsild, P.; Timmusk, T. Regulation of Different Human NFAT Isoforms by Neuronal Activity. *J. Neurochem.* **2016**, *137*, 394–408. [[CrossRef](#)]
69. Yissachar, N.; Sharar Fischler, T.; Cohen, A.A.; Reich-Zeliger, S.; Russ, D.; Shifrut, E.; Porat, Z.; Friedman, N. Dynamic Response Diversity of NFAT Isoforms in Individual Living Cells. *Mol. Cell* **2013**, *49*, 322–330. [[CrossRef](#)]
70. Sreaton, R.A.; Conkright, M.D.; Katoh, Y.; Best, J.L.; Canettieri, G.; Jeffries, S.; Guzman, E.; Niessen, S.; Yates, J.R.; Takemori, H.; et al. The CREB Coactivator TORC2 Functions as a Calcium- and cAMP-Sensitive Coincidence Detector. *Cell* **2004**, *119*, 61–74. [[CrossRef](#)]

71. Puertollano, R.; Ferguson, S.M.; Brugarolas, J.; Ballabio, A. The Complex Relationship between TFEB Transcription Factor Phosphorylation and Subcellular Localization. *EMBO J.* **2018**, *37*, e98804. [[CrossRef](#)]
72. Wu, H. Activation of MEF2 by Muscle Activity Is Mediated through a Calcineurin-Dependent Pathway. *EMBO J.* **2001**, *20*, 6414–6423. [[CrossRef](#)] [[PubMed](#)]
73. Bito, H.; Deisseroth, K.; Tsien, R.W. CREB Phosphorylation and Dephosphorylation: A Ca²⁺- and Stimulus Duration-Dependent Switch for Hippocampal Gene Expression. *Cell* **1996**, *87*, 1203–1214. [[CrossRef](#)] [[PubMed](#)]

Disclaimer/Publisher’s Note: The statements, opinions and data contained in all publications are solely those of the individual author(s) and contributor(s) and not of MDPI and/or the editor(s). MDPI and/or the editor(s) disclaim responsibility for any injury to people or property resulting from any ideas, methods, instructions or products referred to in the content.